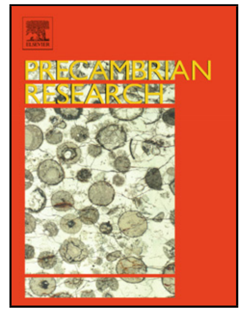

Title: Zircon U-Pb ages and Lu-Hf isotope systematics from late-tectonic granites, Geita greenstone belt: implications for crustal growth of the Tanzania craton

Author: I.V. Sanislav R.J. Wormald P.H.G.M. Dirks T.G. Blenkinsop L. Salamba D. Joseph

PII: S0301-9268(14)00008-4
DOI: http://dx.doi.org/doi:10.1016/j.precamres.2013.12.026
Reference: PRECAM 3907

To appear in: *Precambrian Research*

Received date: 14-6-2013
Revised date: 2-11-2013
Accepted date: 31-12-2013

Zircon U-Pb ages and Lu-Hf isotope systematics from late-tectonic granites, Geita greenstone belt: implications for crustal growth of the Tanzania craton

I.V. Sanislav[a]*, R. J. Wormald[a], P. H. G. M. Dirks[a], T. G. Blenkinsop[a], L. Salamba[b], D. Joseph[b]

[a] Economic Geology Research Unit (EGRU) and School of Earth and Environmental Sciences, James Cook University, Townsville, 4011, QLD, Australia

[b] Geita Gold Mine, Geita, P.O. Box 532, Geita Region, Tanzania

Abstract

Granite plutons that intruded south of lake Victoria and north of the Geita greenstone belt have geochemical characteristics similar to high-K granites. When compared to the late high-K granites from the Musoma-Mara region, they have lower SiO_2 content and higher TiO_2, Al_2O_3, CaO, Na_2O, P_2O_5, MgO and FeO_t. They also show higher values for V, Sr, Zr, Ba and Hf concentrations. All samples display high total REE abundances (ΣREE 139-393) and weak to moderate Eu depletion (Eu/Eu*: 0.25-0.77). Their chondrite-normalized pattern indicates that the light REE are moderately fractionated ($3.03<La_n/Sm_n<6.24$), whereas the heavy REE are weakly fractionated ($1.63<Gd_n/Yb_n<2.80$). The granite plutons are generally undeformed with $^{207}Pb/^{206}Pb$ ages between 2660 and 2620 Ma, and intruded after the main ductile deformation that affected the Geita greenstone belt. The $^{176}Hf/^{177}Hf$ ratios for zircons from all samples are identical within error suggesting evolution from an isotopically uniform reservoir. The ε_{Hf} values plot along the CHUR evolution line indicating that the granite represents juvenile crustal melts derived from greenstone material.

Available zircon ages from the Tanzania Craton suggest that crustal growth occurred in three distinct periods, 2850-2800 Ma, 2770- 2730 Ma and 2700- 2620 Ma, with the dominant period of crustal growth around 2700 Ma. Zircon ages from the Sukumaland and Musoma-Mara greenstone belts indicate that the greenstone sequences formed during the same three periods of crustal growth.

Keywords: Tanzania Craton; Archean granites; zircon ages; Lu-Hf isotopes; crustal evolution

1. Introduction

Archean cratons represent old (>2500 Ma) and stable continental crust characterized by low geothermal gradients and thick lithospheric roots (Artemieva and Mooney, 2001; Artemieva and Mooney, 2002; Petitjean et al., 2006). They are particularly important sections of the Earth crust, because their geology provides important clues about the development and evolution of the earliest solid crust as well as the development of early life on Earth (e.g. Lowe and Tice, 2007; Schopf et al., 2007; Kemp et al., 2010; Adam et al., 2012). The geology of Archean cratons is dominated by two broad lithological categories. The first one consists of granite-greenstone terrains comprising a succession of variably deformed and metamorphosed volcanic and plutonic rocks, mostly mafic in composition, associated sedimentary rocks, typically mudstones, greywacke and ironstones and late granites (e.g. de Witt, 1998; Jelsma and Dirks, 2000; Peschler et al., 2004; Robin and Bailey, 2009). The second category consists mainly of high grade, mostly felsic, gneiss and granulite (e.g. de Witt, 1998; Martin et al., 2005). Their peculiar geology has led to important questions in geology such as: did modern day plate tectonic processes operate in the Archean? Since Archean granite-greenstone terrains do not have a modern day analogue this question has led to heated debate (e.g. Kröner and Layer, 1992; deWit, 1998; Hamilton, 1998, 2003; Smithies et al., 2005, 2007; Cawood et al., 2006; Van Kranendonk, 2007; Korenga, 2013). Although the issue of tectonic setting remains unresolved, it has been noted that the physio-chemical processes that gave rise to the evolution of felsic magmatism in Archaean cratons follows a similar differentiation trend with time in all cratons (e.g. Champion and Smithies, 2001; Martin and Moyen, 2002; Smithies et al., 2003). This secular variation in granite geochemistry starts with early TTG suites, followed by transitional TTG suites and ends with late-tectonic, high-K granites. The emplacement of late-tectonic granites has been correlated, with the genesis of world class gold deposits (e.g. Hagemann and Cassidy, 2000). Therefore, understanding their timing of emplacement is important for both economic and geological reasons.

The Lake Victoria region of the Archean Tanzania Craton contains a series of narrow, linear greenstone belts trending more or less E-W, bordered by gneiss and granite. Recent studies have shown that the gneiss units that border the greenstone belts in the Sukumaland Greenstone Belt do not necessarily represent the basement to the greenstone belt with new ages suggesting that parts of the gneiss terrains are younger than the greenstone belt successions (e.g. Borg and Krogh, 1999, Manya et al., 2006). Kabete et al., (2012a, b) subdivided the Archean Tanzania Craton in a series of WNW-ESE trending terrains, which were interpreted to represent accretionary terranes during growth of the Tanzania Craton. The geological history of individual terrains and their boundaries, and indeed the assumed accretionary process, remains poorly understood.

In this contribution we present new zircon ages and Lu-Hf isotope systematics from late-tectonic granite plutons that intruded the strongly deformed greenstone lithologies of the Geita greenstone belt, directly south of Lake Victoria, and discuss their tectonic significance in relation to existing geochronological data from the Tanzania craton. As part of this execrcise we reinterpret the existing geochronology in terms of crustal growth and evolution of the Tanzania Craton.

2. Regional geology

The Tanzania craton is a late Archean craton that is exposed over most of central and northern Tanzania, western Kenya, and southeastern Uganda, and most likely extends under Lake Victoria. The craton is surrounded by younger mobile belts, the Kibaran, Ubendian and Usagaran belts to the west, south-west and south respectively, and the Mozambique belt to the east (Fig. 1). The Tanzania Craton consists mostly of granitic rocks, which in the northern part of the craton enclose a series of mostly east-west trending greenstone belts (e.g. Manya and Maboko, 2003; Manya et al., 2006; Kabete et al., 2012 a, b).

The stratigraphy of the Tanzania craton has been subdivided in three main units (e.g., Barth, 1990; Kuehn et al., 1990; Borg, 1992; Borg and Shackelton, 1997; Borg and Krogh, 1999). These are, in the order of their assumed relative age: the Dodoman Belt, the Nyanzian Supergroup and the Kavirondian Supergroup. Based on geophysics and remote sensing interpretations, Kabete et al., (2012a) proposed a sub-division of the Tanzania Craton in a number of shear-zone bounded accretionary terranes: the East Lake Victoria, Mwanza-Lake Eyasi, Lake Nyanza, Moyowosi-Manyoni, Dodoma Schist and Dodoma Basement terranes. This interpretation is yet to be confirmed by field, geochronology and geochemistry data.

The Dodoman Supergroup was interpreted to represent the stratigraphically lowermost unit of the Tanzania craton. The Dodoman Supergroup is composed of a granite-migmatite terrain, which contains a series of WNW-ESE trending belts of high- and low-grade supracrustal rocks. The high-grade rocks consist of granulite-facies metamorphics (pyroxene gneiss, hornblende-diopside gneiss) that locally grade into migmatite and are intruded by gabbroic rocks surrounded by biotite-hornblende gneiss, amphibolite, kyanite gneiss and migmatite that have been metamorphosed at almandine-amphibolite facies grade (e.g. Gabert, 1990). The low-grade metamorphics consist of talc-chlorite, sericite and corundum-bearing schists. Some authors (Bell and Dodson, 1981) advanced the hypotheses that the Dodoman and the Nyanzian are coeval. This hypothesis was further supported by a single zircon U-Pb age of 2680±3 Ma from migmatite gneiss near the southern margin of the Sukumaland Greenstone Belt (Borg and Krogh, 1999).

The Nyanzian Supergroup consists of typical greenstone belt assemblages with metamorphosed volcanics, sediments and granites. The greenstone belts occur as irregularly shaped lenses up to 30 kilometers wide and up to several hundred kilometers long. Six different, E-W trending, greenstone belts have been identified in the Tanzania craton. These are: the Sukumaland Greenstone Belt, Shinyanga-Malita Greenstone Belt, Musoma-Mara Greenstone Belt, Kilimafedha Greenstone Belt, Nzega Greenstone Belt and Iramba-Sekenke Greenstone Belt (Borg and Krogh, 1997). The greenstones have been multiply deformed with synclinal structures preserved in most cases. They are generally metamorphosed under greenschist facies conditions, except near granite intrusions where amphibolite facies metamorphism has been recorded. The Sukumaland Greenstone belt, is a complex amalgam of a number of separate greenstone domains surrounded by granite. The Geita greenstone belt, which is the focus of this study, represents a major E-W trending greenstone fragment (70x20 km) along the northern margin of the Sukumuland Greenstone Belt.

In general the stratigraphic base of the Nyanzian Supergroup is composed of mafic, predominantly tholeitic, volcanics (lavas and pillow lavas, tuffs and agglomerate), followed by intermediate and felsic volcanics (andesitic, rhyodacitic and rhyolitic rocks) with associated tuffs and agglomerate, and intercalations of metapelites. This succession is overlain by banded ironstone, felsic tuffs, graphitic shale, chert, quartzite and locally rhyolitic volcanics. The

Nyanzian has been subdivided into the Lower and Upper Nyanzian (e.g., Kuehn et al., 1990; Borg, 1992; Borg and Shackelton, 1997; Borg and Krogh, 1999). The Lower Nyanzian is composed primarily of tholeitic amphibolite and meta-gabrro with minor occurrences of meta-andesite and ultramafic rocks, while the Upper Nyanzian is dominated by banded ironstone, clastic sediment and metavolcanic rocks of rhyolitic composition. Barth (1990) interpreted the Lower Nyanzian succession as a proximal facies and the Upper Nyanzian as a distal facies in relation to the craton hinterland. Borg and Krogh (1999) and Manya and Maboko (2003) point out that similar ages from rocks of the Lower Nyanzian to those of the Uppers Nyanzian suggest a more complex tectono-stratigraphic relationship than that implied by a simple stratigraphic succession.

The Kavirondian Supergroup represents a succession of sedimentary rocks that unconformably overlies the Nyanzian Supergroup. It was interpreted to represent the molasse facies of the greenstone, generally folded on E-W trending axes (e.g. Gabert, 1990). The Kavirondian is composed of conglomerate, quartzite, arkosic and feldspathic grit, sandstone and siltstone, shale, phyllite and tuff. A minimum age of ~2450 Ma and a maximum age of ~2740 Ma are inferred for the Kavirondian (Gabert, 1990).

3. A geochronological framework for the Tanzania Craton

3.1 Magmatic ages

The amount of published igneous ages from the Tanzania Craton is scarce compared to other Archean cratons (e.g. Yilgarn, Superior, Zimbabwe or Kaapvaal Craton; Davis et al., 2005; Griffin et al., 2008; Rollinson and Whitehouse, 2011) of similar age. Most of the available igneous ages come from an unpublished company report (Chamberlain and Tosdal, 2007), though some of this data was included in Kabete et al. (2012a). The oldest zircon igneous age was determined from a granodiorite from the North Mara mine at 2843±12 Ma (Chamberlain and Tosdal., 2007), while the youngest igneous zircon age of 2567±10 Ma comes from a tonalite in the Sarama-Rwamagaza area. A similarly young, Sm-Nd garnet whole rock isochron age, of 2544±15 Ma was reported by Cloutier et al. (2005) for aplitic, leucogranite dykes that crosscut the greenstone succession at the Tulawaka gold deposit. A series of zircon U-Th-Pb ion microprobe ages between 2635±10 Ma and 2676±12 Ma were reported by Manya et al. (2006)

from foliated to massive granitoids from the Musoma Mara Greenstone belt. For granitoids in the Mara region Chamberlain and Tosdal (2007) reported zircon ages older than 2800 Ma, one age at 2743±28 Ma and a few ages between 2660 and 2671 Ma. The only available igneous ages from the Kilimafedha Greenstone Belt were reported by Wirth et al. (2004) from two granite samples dated at 2643±11 Ma and 2692±11 Ma respectively. From the Shinyanga-Malita Greenstone Belt, Chamberlain and Tosdal (2007) reported three zircon ages from two granitoids (one at 2656±11 Ma and one at 2680±9 Ma) and one tonalite (2765±25 Ma) from the Kahama-Mwadui area. They also report a microgranite age of 2640±17 Ma and a granodiorite age of 2655±16 Ma from the Nzega Greenstone Belt, and the only igneous age from the Iramba-Sekenke Greenstone Belt from a diorite at 2751±17 Ma. From the Sukumaland Greenstone Belt, Borg and Krogh (1999) reported a zircon age of 2680±3 Ma from a migmatitic gneiss near Kahama. From the same greenstone belt Chamberlain and Tosdal (2007) reported a similar age (2698±12 Ma) for gneiss near Lubando (east of Geita). From the same area they reported two identical zircon ages of 2743 Ma for a diorite and a gabbro sample; and from near Imweru (west of Geita) another two identical ages at 2758 Ma for two diorite samples. From the Geita area they reported a tonalite age of 2738±9 Ma and a 2666±8 Ma age from a granitoid sample. From near Kasubuya they reported a granodiorite age of 2653±10 Ma and from near Bukoli a granitoid age of 2646±14 Ma. Kabete et al., (2012b) reported a zircon age of 2691±7 Ma for a hornblende granitoid from rocks assigned to the Dodoman basement super-terrane, and a 2681±5 Ma age for a K-feldspar granitoid near Singida.

3.2 Volcanic ages

The ages of the volcanic units range from 2831±7 Ma to 2531±2 Ma (Chamberlain and Tosdal, 2007; Pinna et al., 2000) with the oldest age coming from a rhyolite in the Maji Moto area, Musoma-Mara Greenstone Belt and the youngest age coming from an ignimbrite within the Kisii Group of western Kenya. From the Musoma-Mara Greenstone Belt, Chamberlain and Tosdal (2007) reported two ages above 2800 Ma and one age at 2653±7 Ma from the Kemambo area, two ages around 2690 Ma from a dacite and a volcanic unit near Nyabigena, one age at 2670±5 Ma from the Kuria area and one dacite age at 2657±8 Ma from the Tarime area. From the Suguti area in the same greenstone belt, Mtoro et al., (2009) reported a rhyolite zircon age of 2754±1 Ma and a Sm-Nd age of 2742±18 which are similar to the 2759±9 Ma zircon age reported by Chamberlain and Tosdal (2007) from the same area. Manya et al., (2006) reported a series of zircon ages around 2670 Ma from two high-Mg andesite units (one at 2673±8 Ma and one at 2669±9 Ma) and two dacite flows (one at 2668±30 Ma and one at 2667±8 Ma).

The oldest volcanic age from the Sukumaland Greenstone Belt is a Sm-Nd whole rock age at 2823±44 Ma reported by Manya and Maboko (2003) from a metabasalt from the Rwamagaza area. A similar zircon age of 2821±30 Ma was reported by Chamberlain and Tosdal (2007) from a pyroclastic tuff near Tulawaka. A more precise zircon age of 2808±3 Ma was reported by Borg and Krogh (1999) from rhyolitic pyroclastic rocks which together with a 2780±3 Ma age from similar rocks were interpreted to date the Upper Nyanzian in the region. Chamberlain and Tosdal (2007) reported two similar ages at around 2780 Ma from felsic pyroclastic tuffs. This period of volcanism appears to be followed by a depositional break, and deposition resumes at around 2715 Ma as revealed by two zircon ages from Bulyanhulu gold mine, one for a dacite (2719±16 Ma) and one for a porphyry dyke (2710±10).

From the Geita area Borg and Krogh (1999) reported a 2699±9 Ma age for a trachyandesite, which is similar to the ages reported by Chamberlain and Tosdal (2007) for a quartz porphyry (2697±3 Ma) and a quartz-feldspar porphyry (2695±18 Ma). From the same area Chamberlain and Tosdal (2007) reported a feldspar porphyry age of 2684±21 Ma and a lamprophyre age of 2686±13 Ma, while Borg and Krogh (1999) reported another lamprophyre age at 2644±3 Ma. Near Biharamulo a feldspar dyke was dated at 2670±21 Ma; near Imweru a porphyry dyke was date at 2667±14 and from Kasubuya a flow banded rhyolite was dated at 2654±15 Ma (Chamberlain and Tosdal, 2007).

The few volcanic ages reported by Chamberlain and Tosdal (2007) from Nzega Greenstone Belt show that the earliest recorded volcanic activity started in the Kibiso Hills area at 2725±22 Ma and 2717±10 Ma. They also reported a 2695±12 Ma age for a dacite, a 2680±13 Ma age for a porphyry dyke and a 2675±25 Ma age for a quartz-eye rhyolite.

From the Kilimafedha Greenstone Belt, Wirth et al., (2004) reported two rhyolite ages, one at 2720±5 Ma and one at 2712±5 Ma. The only volcanic age from the Iramba-Sekenke Greenstone Belt is a Sm-Nd whole rock age of 2742±27 Ma determined from tholeitic basalts by Manya and Maboko (2008).

3.3 Detrital/provenance, metamorphic and inherited ages

Detrital age data from Archean sediments are scarce. Chamberlain and Tosdal (2007) reported a series of detrital zircon ages from BIF units, sandstone, argillite and conglomerate. The oldest age of 2718±11 Ma comes from a BIF unit from the Golden Pride gold mine in the Sukumaland Greenstone Belt. From Biharamulo they reported a zircon age from a BIF unit at 2702±8 Ma, and from Geita they reported a zircon age from BIF at 2670±8 Ma. From Bulyanhulu gold mine they reported a zircon age from a sandstone unit at 2659±41 Ma and a zircon age from an argillite at 2665±9 Ma. From the Musoma Mara Greenstone Belt they reported an age of 2678±8 Ma from the Mtama conglomerate unit and an age of 2657±7 Ma from a sandstone unit.

Chamberlain and Tosdal (2007) interpreted a series of zircon ages from Musoma Mara Greenstone belt as metamorphic ages. From the Mrito metamorphics they reported an age of 2843±4 Ma, and from garnet schist near Kegonga village they reported an age of 2830±11 Ma. They also reported two zircon ages from gneiss from South Mara, one at 2799±30 Ma and one at 2773±9 Ma, and a pegmatite age of 2638±33 Ma.

Kabete et al., (2012b) reported the oldest detrital ages in the Tanzania Craton from fuchsitic-sericite schist from the Udewa-Ilangali terrain in the eastern part of the craton, which contain zircon ages between 3604±6 Ma and 4013±4 Ma. The same authors reported an age of 3230±4 Ma from a quartz-diorite schist and an age of 2702±6 Ma from a biotite-quartz-feldspar schist, which they interpreted to represent the age of a precursor terrain. From a porphyritic andesite they separated three different Archean ages, one at 2656±17 Ma, one at 2815±7 Ma and one at 3140±7 Ma, which were interpreted to represent inherited ages derived from different source areas.

3.4 Reworked Archean in mobile belts

The range of Archean ages derived from the surrounding mobile belts is similar to those reported from the craton itself. The oldest age of 3507±5 Ma was reported by Cutten et al. (2006) from saphirine-orthopyroxene gneiss from the Usagara-Ukaguru superterrane together with two younger ages of 2777±4 Ma and 2687±15 Ma. Another MesoArchaean age of 3014±1 Ma was reported by Johnson et al. (2003) from charnockitic gneisses from the Kilindi-Handeni superterrane. From the same rocks they reported a series of ages between 2609 and 2896 Ma; an age of 2700±10 Ma from a garnet-biotite gneiss and an age of 2633±13 Ma from an orthogneiss. From the same terrane Kabete et al. (2012b) reported an age of 2670±18 Ma from a biotite quartz-feldspathic gneiss. Sommer et al. (2005) reported an age of 2765±11 Ma from a tonalitic gneiss and an age of 2680±13 Ma from an orthogneiss. From an anorthosite, Tenczer et al. (2006) reported an age of 2643±16 Ma.

Collins et al. (2004) reported an age of 2959±4 Ma and a younger one of 2678±5 Ma from a mylonitic felsic gneiss within the Usagaran Belt. From the Ulugulu-Pare superterrane Muhongo et al. (2001) reported three zircon ages from granitic gneiss, one at 2740±0.3 Ma, one at 2705±0.3 Ma and one at 2608±0.2 Ma. From the same area Maboko (1995) reported a young age of 2566±9 Ma from a biotite paragneiss, which was interpreted to be a provenance age. From gneiss of the Isimani suite at the southern border of the Tanzania Craton, Reddy et al. (2003, 2004) reported an age of 2698±15 Ma and an age of 2705±11 Ma. From Usagara-Ukaguru superterrane, Sommer et al. (2005) reported a series of ages between 2630 and 2771 Ma from mafic granitoid gneiss, an age of 2650±14 from a trondhjemitic gneiss and an age of 2630±16 Ma from garnet-bearing mafic granitic gneiss. Tenczer et al., (2012) reported a range of Archean zircon ages between 2529 and 2812 Ma and one monazite age at 2610±44 Ma from rocks along the eastern margin of the Tanzania Craton. From Ruaha river, Vogt et al., (2006) reported an age of 2697±5 Ma from a gneiss and an age of 2617±5 Ma from a biotite granite-gneiss.

4. New age and geochemical data for the Geita greenstone belt

4.1 Samples description

Figure 2 shows the geology and sample locations of granites bounding the northern margin of the Geita Greenstone belt, 5-10 km south of Lake Victoria. The granites form an intrusive contact with the northern margin of the Geita Greenstone Belt. Isolated greenstone fragments can be found locally within the granites. The granites are undeformed (except local narrow deformation zones) and in places show a magmatic fabric defined by the alignment of feldspar and/or biotite crystals. The mineralogy of these granites consists mainly of quartz, K-feldspar, plagioclase and biotite. Common accessory minerals include apatite, hornblende, zircon, epidote, titanite, pyrite and magnetite. Four of the samples, GX-01, GP-01, GP-03 and XU-02 are coarse-grained with an equigranular texture while the remaining three samples, GP-02, XU-01 and XU-01A are porphyritic with large euhedral K-feldspar crystals. The larger phenocrysts, up to 5 cm in size, always consist of K-feldspar. Mafic enclaves are observed towards the contact with the greenstone.

4.2 Analytical methods

4.2.1 Major and trace elements

Whole rock samples were split and trimmed to remove the altered surfaces and fresh portions were crushed and milled in a tungsten carbide mill for major and trace element analyses. Major elements were analyzed at the Advance Analytical Centre housed in James Cook University by X-ray fluorescence (XRF) spectroscopy using a Bruker-AXS, S4 Pioneer XRF Spectrometer. Trace element abundances were determined by inductively coupled plasma mass spectrometry using a Varian ICP-MS 820 spectrometer.

4.2.2 Zircon dating and Hf isotopes procedures and protocols

The rocks were split to remove weathered surfaces than milled with a tungsten carbide disc mill to a grain size of ≤ 500 µm. The 500 µm portion was run in a water current on a Wilfley table to collect the heavy mineral fraction, and subsequently run through a Frantz magnetic separator. Separates were obtained from the non-magnetic fraction using heavy liquids from which the heavy fraction was re-run through a Frantz magnetic separator. Zircons were hand-picked from the non-magnetic fraction and mounted into epoxy resin blocks and polished to about half of their thickness; first with a 3 µm diamond paste than with a 1 µm diamond paste. About 40 to 60 zircons were mounted for each sample.

Prior to analysis, zircon grains were imaged using a Jeol JSM5410LV with attached cathodoluminescence detector in order to identify zonational domains and inherited cores within the grains (Fig. 3). U–Pb isotope analyses were obtained using a GeoLas 200 Excimer Laser Ablation System in a He ablation atmosphere, coupled to a Varian ICP-MS 820 series instrument. Laser parameters during the analyses include a repetition rate of 10 Hz, spot size of 40 µm and energy of 6.0 J/cm^2. Analyses involved 30 seconds of background measurement (gas blank) followed by 35 seconds of acquisition of U-Pb isotope data. U–Pb fractionation was corrected using the GJ-1 (ID-TIMS $^{207}Pb/^{206}Pb$ age = 608.5 ± 0.4Ma (Jackson et al., 2004) as the primary standard. FC-1 zircons (ID-TIMS $^{207}Pb/^{206}Pb$ age = 1099.0 ± 0.6Ma (Paces and Miller,

1993) and Tem-2 zircons (ID-TIMS $^{206}Pb/^{238}U$ age = 416.8 ± 1.1Ma (Black et al., 2003) were used as secondary standards. A number of zircon grains were excluded from analysis due to the metamict nature and small size of the grains.

Data were processed using the software package GLITTER™ (Jackson et al., 2004), and age calculations were made using Isoplot (Ludwig, 2003). Over the duration of this study the reported weighted average ages (errors at 95% confidence) for GJ-1 are 608 ± 11 Ma for $^{207}Pb/^{206}Pb$ and 601 ± 3.5 Ma for $^{206}Pb/^{238}U$. FC-1 gives an age of 1106 ± 12 Ma for $^{207}Pb/^{206}Pb$ and 1098.1 ± 9.4 Ma for $^{206}Pb/^{238}U$ and Tem-2 436 ± 16 Ma for $^{207}Pb/^{206}Pb$ and 408.5 ± 3.5 Ma for $^{206}Pb/^{238}U$. Analyses with significant discordance (> 10%) and those with elevated common Pb, where $^{206}Pb/^{204}Pb$ (background corrected) is <1000, were excluded from isotope age regressions. $^{207}Pb/^{206}Pb$ grain ages are used in this paper. Abundances of U and Th were measured using a NIST 610 glass standard in conjunction with internal standardization using the known stoichiometric abundance of Si in zircon.

Analytical protocols for Hf isotope data acquisition are outlined in Kemp et al. (2009). The Hf isotope compositions were acquired with a Thermo-Scientific Neptune multi-collector ICP-MS attached to a Coherent GeoLas 193 nm ArF laser, targeting the same area of the zircons that were previously dated by LA-ICP-MS or the same CL defined growth domain. 60 µm laser beam diameters were used at a 4Hz laser repetition rate. Standard zircons analysed during the study were Mud Tank, Temora 2 and FC1, the latter two to check the isobaric interference corrections for Yb. The average $^{176}Hf/^{177}Hf$ and the 2 sigma errors during the analyses for the standards were: 0.282483 (±0.000004) for Mud Tank, 0.282667 (±0.000025) for Temora 2 and 0.282151 (±0.000006) for FC1. Epsilon Hf (ε_{Hf}) values were calculated using the present day chondritic values of $^{176}Hf/^{177}Hf_{CHUR(0)}$ =0.282785 and $^{176}Lu/^{177}Hf_{CHUR(0)}$ = 0.0336 (Bouvier et al., 2008). For this study we adopted the ^{176}Lu decay constant of 1.867 X 10^{-5} m.y.$^{-1}$ proposed by Soderlund et al. (2004).

4.3. Results

4.3.1 Major and trace elements geochemistry

Bulk chemical analyses of the samples are listed in Table 1. Five of the samples (XU-01, XU-01A, XU-02, GP-02 and GP-03) plot in the granite field and two (GP-01 and GX-01) in the granodiorite field on an Ab-An-Or diagram (Fig. 4a). The SiO_2 content of samples is variable between 63.68 and 76.19 percent. The K_2O/Na_2O ratio varies between 0.92 and 1.94 while the aluminum saturation index (ASI) varies between 0.86 and 1.02 making them part of the metaluminous and sodic to potassic group of granites as shown in Figure 4b. Harker plots of silica versus major elements (Fig. 5) show a consistent negative correlation except for K_2O which shows a positive correlation. Large variations can be observed in FeOt (1.56-4.72%), MgO (0.21-1.26 %) and CaO (0.88-3.43%) values. The ratio FeOt/(MgO+FeOt) is moderate ranging from 0.75 to 0.90.

Trace and REE elements analyses are presented in Table 2. All samples show high total REE abundances (ΣREE 139-393) and weak to moderate Eu depletion (Eu/Eu*: 0.25-0.77) that decreases with the SiO_2 content (Fig. 6a). Regarding their chondrite-normalized pattern (Fig. 6 b), the light REE are moderately fractionated ($3.03<La_n/Sm_n<6.24$) while the heavy REE are weakly fractionated ($1.63<Gd_n/Yb_n<2.80$). Variation diagrams of trace elements versus SiO_2 show negative trends for V, Sr, Y, Zr, Ba, Hf, positive trends for Rb, Pb, Th, U, and no clear trends for Nb and Cs. The contents of the large ion lithophile elements (LILE) Ba, Sr and Rb are generally high, but variable (233-1349 ppm for Ba and 87-549 ppm for Sr; 124-247 ppm for Rb). All samples have a moderate to low Y content of 12.9-25.5 ppm that is higher in the porphyritic granite samples. All samples have moderately high U (2.39-13.2 ppm) and Th (9.02-46.3 ppm) compared to the average Upper Crust (Taylor and McLennan, 1985; Rudnik and Gao, 2004). The Zr content is moderate (127-337 ppm) and decreases with the amount of silica with the highest values occurring in the porphyritic granites. The transition elements show low values for Sc (2.69-10.1 ppm), V (40.3-87.4 ppm), Ni (4.07-11.1 ppm) and Cu (2.65-8.96 ppm) and high values for Co (27.3-48.5 ppm) when compared to the average Upper Crust.

4.3.2 Geochronology

Table 3 and Figure 7 show the zircon ages for the seven granite samples north of the Geita greenstone belt. Only analyses with low common lead concentrations were used for the age calculation. The calculated $^{207}Pb/^{206}Pb$ ages for individual samples range from 2617±11 to 2661±14 Ma with an average age for all samples of 2636±6 Ma. Sample XU-01 contains large amounts of elongated euhedral to subhedral zircon grains with low luminescence and brownish color indicating high U contents. The zoning of all zircon grains is concentric reflecting a magmatic origin. The age data is presented in Table 3. The $^{207}Pb/^{206}Pb$ weighted average age (Fig. 7a) for 15 analyzed spots with the lowest common lead concentration is 2617±11 Ma with individual spot ages ranging from 2576±22 Ma to 2657±22 Ma. The upper concordia intercept age for these analyses is 2638±16 Ma (Fig. 7b). The $^{207}Pb/^{206}Pb$ weighted average age for 10 analyses that have less than 10% discordance is 2630±13 Ma and the most concordant analysis yields an age of 2642±19 Ma. The upper concordia intercept for these analyses is 2633±16 Ma. The $^{207}Pb/^{206}Pb$ ratio for all of the selected spots varies very little between 0.17 and 0.18.

All zircon grains from sample XU-01A are brownish in color suggesting high U content and have an elongated euhedral to subhedral shape with concentric zoning indicating a magmatic origin. The $^{207}Pb/^{206}Pb$ weighted average age (Fig. 7c) for 11 analyzed spots with the lowest common lead concentration is 2628±12 Ma with individual spot ages ranging between 2612±19 Ma and 2637±18 Ma. The upper concordia intercept age for these spots 2630±8 Ma (Fig. 7d). The $^{207}Pb/^{206}Pb$ weighted average age for the analyses with less than 10% discordance is 2627±12 Ma and the upper concordia intercept age for these analyses is 2630±8 Ma. The $^{207}Pb/^{206}Pb$ ratio for the selected spots is constant at 0.17.

The zircon grains in sample XU-02 are dominantly elongated with euhedral shape and brownish colour suggesting high U contents. Their concentric zoning points towards a magmatic origin. The $^{207}Pb/^{206}Pb$ weighted average age (Fig. 7e) for 6 analyzed spots with the lowest common lead concentration is 2623±15 Ma with individual spot ages ranging between 2612±17 Ma and 2658±20 Ma. The upper concordia intercept age for these spots is 2620±35 Ma (Fig. 7f). The $^{207}Pb/^{206}Pb$ weighted average age for three analyses with less than 10% discordance is 2614±20 Ma and the upper concordia intercept age for these analyses is 2617±17 Ma. The $Pb/^{206}Pb$ ratio for the selected spots varies very little between 0.17 and 0.18.

Most zircon grains from sample GP-01 are short with euhedral to subhedral shapes with a few elongated grains. They are mostly brownish in colour suggesting high U contents. The $^{207}Pb/^{206}Pb$ weighted average age (Fig. 7g) for 13 analyzed spots with the lowest common lead concentration and with less than 10% discordance is 2652±10 Ma with individual spot ages ranging from 2626±18 Ma to 2694±18 Ma. The upper concordia intercept age for these analyses is 2658±14 Ma (Fig. 7h). The $^{207}Pb/^{206}Pb$ ratio for the selected spots varies little between 0.17 and 0.18.

Sample GP-02 contains mainly elongated euhedral to subhedral zircon grains with concentric zoning indicating a magmatic origin, and a brownish color suggests high U content. The

$^{207}Pb/^{206}Pb$ weighted average age (Fig. 7i) for 9 analyzed spots with the lowest common Pb concentration is 2634±41 Ma with individual spot ages ranging between 2604±70 Ma and 2655±81 Ma. The upper concordia intercept age for these analyses is 2637±43 Ma (Fig. 7j). The $^{207}Pb/^{206}Pb$ weighted average age for analyses with less than 10% discordance is 2637±45 Ma and the upper concordia intercept age is 2634±51 Ma. The $^{207}Pb/^{206}Pb$ ratio for the selected spots varies little between 0.17 and 0.18.

Sample GP-03 contains a mix of short and elongated zircon grains with euhedral to subhedral shapes and concentric zoning with a brownish color indicating high U contents. The $^{207}Pb/^{206}Pb$ weighted average age (Fig. 7k) for 7 analyzed spots with the lowest common Pb and less than 10% discordance is 2661±14 Ma with individual spot ages ranging between 2620±20 Ma and 2681±18 Ma. The upper concordia intercept age for these analyses is 2648±16 Ma (Fig. 7l). The most concordant analyses has a $^{207}Pb/^{206}Pb$ age of 2661±18 Ma. The $^{207}Pb/^{206}Pb$ ratio for the selected spots varies from 0.17 to 0.18.

Sample GX-01 has undergone significant Pb loss and the isotopic system was disturbed. The zircon grains in this sample are mainly elongated with euhedral to subhedral shapes, concentric zoning and a brownish color. One analysis with less than 10% discordance has a $^{207}Pb/^{206}Pb$ age of 2630±27 Ma and one analysis with no common Pb, but with a 14% discordance has a $^{207}Pb/^{206}Pb$ age of 2638±24 Ma. These ages are similar within error to the upper intercept concordia age of 2642±32 Ma (Fig. 7m) calculated for 17 analyses with the lowest common Pb content.

4.3.3 Lu-Hf zircon results

During this study Lu-Hf isotope analyses were performed on cores and rims of 29 zircon grains from 7 samples. The Lu-Hf isotope compositions of zircons from the various samples are shown in Table 4. Corfu and Noble (1992) have shown that zircon fractions from uniform age populations with less than 10% discordance have indistinguishable Hf isotopic ratios. In the present study most of the Hf isotopic measurements were done on zircons with less than 10% discordance, therefore, most likely, they represent primary values. Present-day $^{176}Hf/^{177}Hf$ in the analyzed zircons ranges from 0.281085 to 0.281276 with an average of 0.281139±0.000038 while $^{176}Lu/^{177}Hf$ ranges from 0.00019 to 0.00306 with an average of 0.00085±0.00047. Due to low $^{176}Lu/^{177}Hf$ ratios observed for the zircons, in-situ radiogenic growth over the ca. 2640 Ma life of the zircons must account for only a small fraction of the observed variation in present day $^{176}Hf/^{177}Hf$, the remainder of which must be due to the initial Hf isotope composition of the zircons. Time corrected $^{176}Hf/^{177}Hf$ ratios vary between 0.281056 and 0.281168 (Fig. 8a), with an average of 0.281096±0.000021 and the initial ε_{Hf} values of these zircons range from 2.88 to -0.92 (Fig. 8b) with an average of 0.29±0.7. These narrow ranges (Figs. 8 a, b) point toward a fairly uniform isotopic composition of the source magma. Higher values obtained from some of the metamict cores may be an artifact of the age uncertainty due to localized Pb loss, or alternatively may suggest the presence of a more mafic component in the early stages of crystallization. Figure 8c and 8d show plots of $^{176}Hf/^{177}Hf$ and ε_{Hf} versus the corresponding crystallization age. All samples plot above the CHUR evolution line and the majority of ε_{Hf} values are close to the CHUR value of 0 indicating a crustal component in the source rock of these magmas. The depleted mantle Hf model ages for all samples are close to 2900 Ma while CHUR model ages are almost identical with the $^{207}Pb/^{206}Pb$ ages suggesting a juvenile crustal source with some minor mantle contributions. We note that model ages from crustal derived melts should be interpreted with care since they may represent an average contribution of the involved sources.

5. Discussion

5.1 Implications for the tectonic evolution of the Geita greenstone belt.

The granites that occur to the north of the Geita greenstone belt are undeformed and transect strongly sheared and folded greenstone sequences, suggesting that their timing postdates the main phase of deformation in the region. This suggests that the granitoids were emplaced during the waning stages of late Archean deformation in the area. The maximum age of ca. 2660 Ma recorded by these granites provides a minimum age estimate for the end of the main tectonic phase that affected this part of the Tanzania Craton, while the minimum age of ca. 2620 Ma may record the end of plutonic and tectonic activity in the region. These new ages indicate that the age of post-kinematic intrusions into the Lake Nyanza Superterrane (Kabete et al., 2012 a) is about 40 Ma younger than previously assumed (Kabete et al., 2012 b).

Figure 9a shows the distribution of plutonic ages in the Sukumaland Greenstone Belt and adjacent areas, from which the existence of at least two distinct periods of plutonic activity can be inferred. The first period took place between 2760 and 2730 Ma and was characterized by mafic to intermediate plutonism. These intrusions are spatially located within the greenstone belts and most probably are part of the greenstone succession. The second period of plutonism occurred between 2700 and 2620 Ma and appears to be dominated by the intrusion of felsic plutons. This range of ages occurs within the greenstone belts, in the gneiss terrain and within the granite terrain suggesting widespread magmatic activity rather than magmatic activity concentrated along individual belts. One young age of 2567 Ma (Chamberlain and Tosdal, 2007) is difficult to interpret since ages younger than 2600 Ma are rare within the Tanzania Craton. Figure 9b shows the distribution of volcanic ages within the Sukumaland Greenstone Belt. One distinct period of volcanism can be distinguished between 2840 and 2770 Ma and possibly another one between 2720 and 2640 Ma. The second period of volcanism is uncertain due to ambiguity in rocks description. The gap in volcanic activity between 2770 and 2720 Ma corresponds to the oldest plutonic activity recorded in the region. The only available detrital ages indicate sedimentation took place between 2700 and 2660 Ma, which corresponds to the second period of volcanic and plutonic activity. It can be interpreted that two periods of greenstone deposition took place: one between 2830 and 2770 Ma dominated by volcanic sequences and followed by mafic to intermediate plutonism, and one between 2720 and 2660 Ma dominated by volcano-sedimentary sequences followed by felsic plutonism.

A comparison with the Musoma-Mara region may provide a better understanding of the evolution of the northern part of the Tanzania Craton. Figure 9c and 9d shows three periods of plutonism and volcanism in the Musoma-Mara region. The first period of plutonism occurred between 2850 and 2800 Ma, synchronous to the first period of volcanism that occurred between 2830 and 2800 Ma in the Sukumaland greenstone Belt. The second period of synchronous volcanic and plutonic activity in the Musoma-Mara region occurred between 2760 and 2740 Ma, during the period of oldest plutonic activity and the gap in volcanism in the Sukumaland region. The last period of volcanism in the Musoma-Mara region occurred between 2700 and 2650 and the last period of plutonism occurred between 2700 and 2630 Ma, i.e. Similar to those recorded in the Sukumaland region. The apparent lack of plutonic ages older than 2800 Ma in the Sukumaland region and the apparent gap of volcanic ages between 2770 and 2720 Ma in the Sukumaland region may reflect sampling bias rather than temporally distinct events. However, Manya et al. (2007), based on the geochemistry of high-Mg andesite and associated adakite proposed that the Musoma-Mara region formed in a continental margin setting while Barth (1990), Manya (2001) and Manya and Maboko (2003) proposed that the Sukumaland region formed in an intra-oceanic setting. Manya et al. (2006) not only suggested that the greenstone belts in the Lake Victoria region formed in different tectonic settings but also during different periods of time. The currently available age data suggest a rather common temporal development for the entire Lake Victoria region of the Tanzania craton. Whether or not the greenstone belts represent individual depositional basins, or accretionary terranes, each with an independent evolution, or a single stratigraphic sequence fragmented by the diapiric ascent of gneiss domes and the intrusion of large granite bodies (e.g. Dirks and Jelsma, 1998; van Kranendonk et al., 2007; Korenda, 2013) it is subject to further work.

5.2 The age and crustal growth of the Tanzania Craton

The distribution of available magmatic and volcanic ages (Figures 10a, b;) from the Tanzania Craton indicate three major periods of crustal growth, one between 2850 and 2800 Ma, one between 2770 and 2730 Ma and one between 2700 and 2620 Ma, which are similar to those identified for the Lake Victoria region (see above). This data set is strongly biased towards a larger contribution of geochronological data from the Lake Victoria region. The two young ages of ~2550 Ma (Pinna et al., 2000; Chamberlain and Tosdal, 2007) may reflect a late post-tectonic thermal event that locally affected the Tanzania Craton, or could represent poor data. The distribution of the age data also suggests that the main phase of crustal growth occurred after 2700 Ma. The Archean ages reported from reworked Archean sequences (Figure 10c), which are now part of the mobile belts surrounding the Tanzania Craton show a similar age distribution with most of the ages in the range 2800-2600 Ma, and with peak crustal growth post 2700 Ma. Detrital zircons of Archean age separated from the surrounding rift basins show a similar age distribution between 2800 and 2600 Ma with the majority of ages concentrated between 2700 and 2600 Ma (E. Roberts – personal communication). A few ages suggest the presence of older crust of 3000 to 3600 Ma probably derived from the Tanzania Craton itself. This possibility is further supported by ages of 3230 Ma from metamorphosed quartz-diorite schist, which were interpreted to represent the minimum age of the precursor igneous rock, and by detrital ages from fuchsitic-sericite schist showing an age population between 3600 and 4200 Ma (Kabete et al., 2012b). The crystal shape and the internal zoning of the 4000 Ma zircons separated from the fuchsitic schist indicate deposition close to the source suggesting that these zircon grains may have been sourced from the Tanzania Craton itself (J. Kabete – personal communication). Overall, the existing geochronological data suggest that the Tanzania craton was built between 2850 Ma and 2620 Ma with peak crustal growth between 2700 Ma and 2650 Ma (Fig. 10d), which coincides with a major worldwide period of crustal growth (Condie, 2005).

5.3 The geochemistry of the granites

The geochemistry of the late Archean granites that outcrop to the north of the Geita greenstone belt show several differences when compared to the late Archean granites from the Musoma-Mara region (Manya et al., 2007; Mshiu and Maboko, 2012). The granites in the Geita area are characterized by lower SiO_2 content and higher TiO_2, Al_2O_3, CaO, Na_2O, P_2O_5, MgO and FeO_t (Fig. 5). The trace element concentrations (Fig. 11) show higher values for V, Sr, Zr, Ba and Hf while the chondrite normalized REE (Fig. 6b) show a similar pattern to the granites from Musoma-Mara region.

While all the granites from the Musoma-Mara region plot into the granite field the samples collected from the Sukumaland region plot into the granite to granodiorite field. When plotted on the tectonic setting discrimination diagram the two groups of granites plot in the fields of syn-collisional and volcanic arc granites suggesting petrogenesis in a similar tectonic setting. Similarities and differences between the late Archean granites from the Sukumaland region and the ones from the Musoma-Mara region suggest that the former were most probably derived by melting of earlier TTG-dominated crust or greenstone material. This is consistent with the U-Pb and Lu-Hf isotopic evidence which suggest that the granitoids north of the Geita greenstone belt are derived from a homogeneous $^{176}Hf/^{177}Hf$ source. Their calculated εHf values (-0.91 to 2.88) plot lower than the depleted mantle (Fig. 8d) evolution curve and suggest that they are not juvenile mantle melts, but most probably formed by melting of ≤ 2700 Ma crust.

5. Acknowledgements

The authors would like to acknowledge sponsorship by Geita Gold Mine and Anglogold Ashanti. James Cook University is acknowledged for providing access to the superb analytical facilities located at the Advance Analytical Centre. Many thanks to Sergio Kolling, exploration manager at Geita Gold Mine for numerous discussions about the geology of Geita region which, greatly improved our understanding of the area.

6. References

Adam, J., Rushmer, T., O'Neil, J., and Francis, D., 2012. Hadean greenstones from the Nuvvuagittuq fold belt and the origin of the Earth's early continental crust. Geology *40,* 363–366.

Artemieva, I. M., and Mooney, W. D., 2001. Thermal structure and evolution of Precambrian lithosphere: A global study. Journal of Geophysical Research 106, 16387-16414.

Artemieva, I. M., and Mooney, W. D., 2002. On the relation between cratonic lithosphere thickness, plate motions, and basal drag. Tectonophysics 358, 211-231.

Barth, H., 1990. Provisional Geological Map of Lake Victoria Gold Fields, Tanzania 1:500000 (with explanatory notes). Geologisches Jahrbuch B 72, 59 p.

Bell, K., Dodson, M.H., 1981. The geochronology of the Tanzanian Shield. Journal of Geology 89, 109–228.

Black, L.P., Kamo, S.L., Williams, I.S., Mundil, R., Davis, D.W., Korsch, R.J., Foudoulis, C., 2003. The application of SHRIMP to Phanerozoic geochronology; a critical appraisal of four zircon standards. Chemical Geology 200, 171-188.

Borg, G., 1992. New aspects on the lithostratigraphy and evolution of the Siga Hills, an Archaean granite-greenstone terrain in NW-Tanzania. Zeitschrift fur Angewandte Geologie 38 (2), 89-93.

Borg, G., Shackleton R.M., 1997. The Tanzania and NEZaire Cratons. In: de Wit, M.J., Ashwal, L.D. (Eds.) Greenstone Belts. Clarendon Press, Oxford, pp. 608-619.

Borg. G., Krogh, T., 1999. Isotopic age data of single zircons from the Archaean Sukumaland Greenstone Belt, Tanzania. Journal of African Earth Sciences 29, 301-312

Bouvier, A.,Vervoort, J.D., and Patchett, P.J., 2008. The Lu-Hf and Sm-Nd isotopic composition of CHUR: constraints from unequilibrated chondrites and implications for the bulk composition of terrestrial planets. Earth and Planetary Science Letters 273, 48-57.

Cawood, P. A., Kröner, A., and Pisarevsky, S., 2006. Precambrian plate tectonics:criteria and evidence. GSA Today 16, 4–11.

Chamberlain, C.M., Tosdal, R.M., 2007. U–Pb geochronology of the Lake Victoria Greenstone Terrane, Tanzania. Mineral Deposit Research Unit The University of British Columbia (Research Program on World-class Gold Deposits and Advanced Exploration Projects Owned and/or Joint Ventured to Barick Gold, Placer Dome, Anglo-Gold Ashanti, Resolute Mining NL as Main Sponsors.

Champion, D.C., Smithies, R.H., 2001. Archaean granites of the Yilgarn and Pilbara cratons, Western Australia. *In:* K.F. Cassidy, J.M. Dunphy and M.J. Van Kranendonk (Eds.), 4th Internat. Archaean Symp. 2002; Extended abstracts, AGSO Geoscience Australia, Record 2001/37, pp.134-136.

Cloutier, J., Stevenson, R. K., Bardoux, M., 2005. Nd isotopic, petrologic and geochemical investigation of the Tulawaka East gold deposit, Tanzania Craton. Precambrian Research 139, 147-163.

Collins, A.S., Reddy, S.M., Buchan, C., Mruma, A.H., 2004. Temporal constraints on Palaeoproterozoiceclogite formation and exhumation (Usagaran Orogen, Tanzania). Earth planet Science Letter 224, 175–192.

Condie, K.C., 2005. Earth as an evolving planetary system: Amsterdam, Elsevier, 447 p.

Corfu, F., Noble, S.R., 1992. Genesis of the southern Abitibi greenstone belt, Superior province, Canada: evidence from zircon Hf isotopic analyses using a single filament technique. Geochimica and Cosmochimica Acta 56, 2081–2097.

Cutten, N.H.C., Johnson, S.P., DeWaele, B., 2006. Protolith ages and timing of metasomatism related to formation of white schists at Mautia Hill Tanzania: implications for the assembly of Gondwana. Journal of Geology 114, 683–698.

Davis, D.W., Amelin, Y., G.M. Nowell, and Parrish, R.R., 2005. Hf isotopes in zircon from the western Superior province, Canada: Implications for Archean crustal development and evolution of the depleted mantle reservoir. Precambrian Research 140, 132-156.

de Wit, M.J., 1998. On Archean granites, greenstones, cratons and tectonics: does evidence demand a verdict? Precambrian Research 91, 181–226.

Foley, S.F., Tiepolo, M., and Vannucci, R., 2002. Growth of early continental crust controlled by melting of amphibolite in subduction zones. Nature 417, 637– 640.

Gabert, G., 1990. Lithostratigraphic and Tectonic Setting of Gold Mineralization in the Archean Cratons of Tanzania and Uganda, East Africa. Precambrian Research 46, 59-69.

Hagemann S.G., Cassidy K.F., 2000. Archean orogenic lode gold deposits. Reviews in Economic Geology 13, 9–68.

Hamilton, W.B., 2003. An alternative Earth: GSA Today 13, 4–12.

Hamilton,W.B., 1998. Archean magmatism and deformation were not products of plate tectonics. Precambrian Research 91, 143–179.

Jackson, S.E., Pearson, N.J., Griffin, W.L., Belousova, E.A., 2004. The application of laser ablation-inductively coupled plasma-mass spectrometry to in situ U-Pb zircon geochronology. Chemical Geology 211, 47–69.

Jelsma, H.A., and Dirks, P.H.G.M., 2000. Tectonic evolution of a greenstone sequence in northern Zimbabwe: Sequential early stacking and pluton diapirism. Tectonics 19.

Johnson, S.P., Cutten, H.N.C., Muhongo, S., De Waele, B., 2003. Neoarchean magmatism and metamorphism of the western granulites in the central domain of the Mozambique belt, Tanzania: U–Pb SHRIMP geochronology and PT estimates. Tectonophysics 375, 125–145.

Kabete, J.M., Groves, D.I., McNaughton, N.J., Mruma, A.H., 2012. A new tectonic and temporal framework for the Tanzanian Shield: implications for gold metallogeny and undiscovered endowment. Ore Geology Reviews 48, 88-124.

Kabete, J.M., McNaughton, N.J., Groves, D.I., Mruma, A.H., 2012. Reconnaissance SHRIMP U–Pb zircon geochronology of the Tanzania Craton: Evidence for Neoarchean granitoid–greenstone belts in the Central Tanzania Region and the Southern East African Orogen. Precambrian Research 216– 219, 232– 266.

Kemp, A. I. S., Wilde, S. A., Hawkesworth, C. J., Coath, C. D., Nemchin, A., Pidgeon, R.T., Vervoort, J. D., and DuFrane, A., 2010. Hadean crustal evolution revisited: new constraints from Pb-Hf isotope systematics of the Jack Hills zircons. Earth and Planetary Science Letters 296, 45-56.

Kemp, A.I.S., Foster, G.L., Schersten, A., et al., 2009. Concurrent Pb–Hf isotope analysis of zircon by laser ablation multi-collector ICP-MS, with implications for the crustal evolution of Greenland and the Himalayas. Chemical Geology 261, 244–260.

Korenaga J., 2013. Initiation and Evolution of Plate Tectonics on Earth: Theories and Observations, Annual Review of Earth and Planetary Sciences, 41, 1, 117.

Kröner, A., Layer, P.W., 1992. Crust formation and plate motion in the Early Archean. Science 256, 1405–1411.

Kuehn, S., Ogola, J., Sango, P., 1990. Regional setting and nature of gold mineralization in Tanzania and southwest Kenya. Precambrian Research 46, 71-82.

Lowe, D. R., and M. M. Tice., 2007. Tectonic controls on atmospheric, climatic, and biological evolution 3.5–2.5 Ga. Precambrian Research 158,177–197.

Ludwig, K.R., 2003. User's Manual for Isoplot 3.00. A Geochronological Toolkit for Microsoft Excel. Berkley Geochronology Centre Special Publication No.4.

Maboko, M.A.H., 1995. Neodymium isotopic constraints on the protolith ages of rocks involved in Pan-African tectonism in the Mozambique Belt of Tanzania. Journal of Geological Society of London 152, 911–916.

Manya, S., 2001. Geochemical investigation of Archaean greenstones in the Rwamagaza area, north-western Tanzania. M.Sc. Thesis, University of Dar-es-Salaam.

Manya, S., Kobayashi, K., Maboko, M.A.H., Nakamura, E., 2006. Ion microprobe zircon U-Pb dating of the late Archean metavolcanics and associated granites of the Musoma-Mara

Greenstone Belt, Northeast Tanzania: Implications for the geological evolution of the Tanzanian Craton. Journal of African Earth Sciences 45, 355-366.

Manya, S., Maboko, M.A.H., 2003. Dating basaltic volcanism in the Neoarchaean Sukumaland Greenstone Belt of the Tanzania Craton using the Sm–Nd method: implications for the geological evolution of the Tanzania Craton. Precambriam Research 121, 35-45.

Manya, S., Maboko, M.A.H., 2008. Geochemistry of the Neoarchaean mafic volcanic rocks of the Geita area, NW Tanzania: implications for stratigraphical relationships in the Sukumaland greenstone belt. Journal of African Earth Sciences 52, 152–160.

Manya, S., Maboko, M. A. H., Nakamura, E., 2007a. Geochemistry and Nd-isotpic composition of potassic magmatism in the Neoarchaean Musoma-Mara Greenstone Belt, northern Tanzania. Precambrian research 159, 231 – 240.

Manya, S., Maboko, M.A.H., Nakamura, E., 2007b.The geochemistry of high-Mg andesite and associated adakitic rocks in the Musoma-Mara Greenstone Belt, northern Tanzania: possible evidence for Neoarchaean ridge subduction?. Precambrian Research 159, 241–259.

Martin, H., Moyen, J.-F., 2002. Secular changes in TTG composition as markers of the progressive cooling of the Earth. Geology 30 , 319– 322.

Martin, H., Smithies, H., Rapp, R. P., Champion, D., and Moyen, J. F., 2005. An overview of the TTG/adakite/sanukitoid relationship and implications for continental crust genesis and evolution. Lithos 79, 1-24.

Mshiu, E.E., and Maboko,M.A.H., 2012. Geochemistry and petrogenesis of the late Archaean high-K granites in the southern Musoma-Mara Greenstone Belt: Their influence in evolution of Archaean Tanzania Craton. Journal of African Earth Sciences 66, 1-12.

Mtoro, M., Maboko, M.A.H., Manya, S., 2009. Geochemistry and geochronology of the bimodal volcanic rocks of the Suguti area in the southern part of the Musoma-Mara Greenstone Belt, Northern Tanzania. Precambrian research 174, 241-257.

Muhongo, S., Kröner, A., Nemchin, A.A., 2001. Single zircon evaporation and SHRIMP ages for granulite-facies rocks in the Mozambique belt of Tanzania. Journal of Geology 109, 171–189.

Paces, J.B., Miller, J.D., 1993. Precise U–Pb ages of the Duluth Complex and related mafic intrusions, northeastern Minnesota: geochronological insights to physical, petrogenetic, paleomagnetic, and tectonomagmatic processes associated with the 1.1 Ga midcontinent rift system. Journal of Geophysical Research 98, 13997–14013.

Peschler, A. P., Benn, K., and Roest, W. R., 2004.Insights on Archean continental geo-dynamics from gravity modeling of granite-greenstone terranes. Journalof Geodynamics 38,185–207.

Petitjean, S., Rabinowicz, M., Grégoire, M. and Chevrot, S., 2006. Differences between Archean and Proterozoic lithospheres: Assessment of the possible major role of thermal conductivity. Geochemistry Geophysics Geosystems 7.

Pinna, P., Cocherie, A., Thieblemont, D., Jezequel, P., 2000. The Kisii Group of western Kenya: An end-Archaean (2.53 Ga) late orogenic volcano sedimentary sequence. Journal of African Earth Sciences 30, 79– 97.

Reddy, S.M., Collins, A.S., Mruma, A.H., 2003. Complex high-strain deformation in the Usagaran Orogen Tanzania: structural setting of Paleoproterozoic eclogites. Tectonophysics 375, 101–123.

Robin, C. M. I., and Bailey, R. C., 2009. Simultaneous generation of Archean crust and sub-cratonic roots by vertical tectonics. Geology 37, 523–526.

Rudnick, R.L., Gao, S., 2004. Composition of the continental crust. *In* Rudnick, R. (Ed.), Treatise on Geochemistry (Vol. 3): The Crust: Amsterdam (Elsevier), 1–64.

Schopf, J. W., Kudryavtsev, A. B., Czaja, A. D., and Tripathi, A. B., 2007. Evidence of Archean life: Stromatolites and microfossils. Precambrian Research 158, 141-155.

Smithies, R.H., Champion, D.C., Cassidy, K.F., 2003. Formation of Earth’s early Archaean continental crust. Precambrian Research 127, 89– 101.

Smithies, R.H., Champion, D.C., Van Kranendonk, M.J., Howard, H.M., Hickman, A.H., 2005. Modern-style subduction processes in the Mesoarchaean: Geochemical evidence from the 3.12 Ga Whundo intra-oceanic arc. Earth and Planetary Science Letters 231, 221–237.

Smithies, R.H., Van Kranendonk, M.J., Champion, D.C., 2007. The Mesoarchean emergence of modern-styles subduction. Gondwana Research 11, 50–68.

Söderlund, U., Patchett, P., Vervoort, J., and Isachsen, C.,2004). The decay constant of ^{176}Lu determined from Lu-Hf and U-Pb isotope systematics of terrestrial Precambrian high-temperature mafic intrusions. Earth and Planetary Science Letters, 219, 311-324.

Sommer, H., Kröner, A., Muhongo, S., Hauzenberger, C., 2005. SHRIMP zircon ages for post-Usagaran granitoid and rhyolitic rocks from the Paleoproterozoic terrain of southwestern Tanzania. South African Journal of Geology 108, 247–256.

Sun, S.S., McDonough, W.F., 1989. Chemical and Isotopic systematics of oceanic basalts: implications for mantle composition and processes. In: Saunders, A.D., Norry, M.J. (Eds.), Magmatism in Oceanic Basins. Geol. Soc. London, Spec. Publ. 42, pp. 313–345.

Taylor S. R., McClennan S. M., 1985. The Continental Crust: Its Composition and Evolution. Blackwell, Oxford. 312 pp.

Tenczer, V., Hauzenberger, C., Fritz, H., Hoinkes, G., Muhongo, S., Klötzli U., 2012. Crustal age domains and metamorphic reworking of the deep crust in Northern-Central Tanzania: a U/Pb zircon and monazite age study. Mineralogy and Petrology, DOI 10.1007/s00710-012-0210-1

Tenczer, V., Hauzenberger, C.A., Fritz, H., Whitehouse, M.J., Mogessie, A., Wallbrecher, E., Muhongo, S., Hoinkes, G., 2006. Anorthosites in the Eastern Granulites of Tanzania—New SIMS zircon U–Pb age data, petrography and geochemistry. Precambrian Research 148, 85–114.

Van Kranendonk, M.J., 2007. Tectonics of early Earth. In: Van Kranendonk, M.J., Smithies, R.H., Bennett, V.C. (Eds.), Earth's Oldest Rocks. Elsevier, pp. 1105–1116.

Vogt, M., Kroner, A., Poller, U., Sommer, H., Muhongo, S., Wingate, M.T.D., 2006. Archean and Paleoproterozoic gneisses reworked during a Neoproterozoic (Pan-African) high-grade event in the Mozambique belt of East Africa: structural relationships and zircon ages from the Kidatu area, central Tanzania. Journal of African Earth Sciences 45, 139–155.

Wirth, K. R., Vervoort, J. D., Weisberger, B., 2004. Origin and evolution of Kilimafedha Greenstone Belt, eastern Tanzania craton: evidence from Nd and Pb isotopes. Geological Society of America Abstracts with Programs 36, 224.

Highlights:

- The granites south of Lake Victoria were emplaced between 2660 and 2620 Ma
- They have geochemical characteristics similar to high-K granites
- Their zircon Lu-Hf signature indicate a uniform isotopic reservoir characteristic of juvenile crustal melts
- The emplacement of high-K granites marks the end of tectonic activity in the region

Sample/Oxides	**GX-01**	**GP-01**	**GP-02**	**GP-03**	**XU-01**	**XU-01A**	**XU-02**
SiO_2	68.11	63.68	68.85	73.3	69.65	68.48	76.19
TiO_2	0.55	0.76	0.64	0.29	0.6	0.66	0.31
Al_2O_3	14.93	16.11	14.48	13.82	14.25	14.45	11.63
FeO	3.45	4.72	3.41	1.56	3.33	3.83	1.81
MnO	0.05	0.07	0.05	0.03	0.05	0.05	0.03
MgO	1.03	1.56	0.66	0.47	0.59	0.73	0.21
CaO	2.67	3.43	2.25	1.31	1.96	2.06	0.88
Na_2O	3.85	4.03	3.63	3.66	3.64	3.58	2.79
K_2O	3.91	3.73	4.71	4.71	4.89	5.12	5.37
P_2O_5	0.16	0.25	0.16	0.05	0.15	0.17	0.06
SO_3	0.01	0.02	0.03	0	0	0.01	0
LOI	1	1.14	0.74	0.51	0.56	0.66	0.45
Total	99.73	99.5	99.63	99.71	99.68	99.81	99.72
Feo/FeO+MgO	0.77	0.75	0.84	0.77	0.85	0.84	0.90
ASI	1.00	1.02	0.95	0.97	0.94	0.93	0.87
K_2O/Na_2O	1.02	0.93	1.30	1.29	1.34	1.43	1.92

Sample/Element	GX-01	GP-01	GP-02	GP-03	XU-01	XU-01A	XU-02
Sc	7.48	10.1	7.47	4	6.75	7.56	2.69
V	67.6	87.4	57.5	40.3	54.8	58	35.7
Mn	379	478	347	201	332	408	166
Co	33.8	35.4	48.5	36.2	28.6	27.3	42.7
Ni	7.67	11.1	5.03	8.18	4.48	4.77	4.07
Cu	7.79	8.96	5.85	5.4	3.57	6.66	2.65
Zn	34.9	50	41.4	20.2	38.5	52.3	20.8
Ga	16.1	16.8	17.4	13.1	17.5	17.8	14.2
Rb	132	124	177	190	179	247	209
Sr	404	549	273	169	232	247	87
Y	12.9	16.3	25.5	14.1	23.4	25.3	21.9
Zr	213	264	314	127	275	337	166
Nb	8.81	8.5	17.9	9.25	16.9	17	11.7
Sn	6.99	6.83	5.74	7.45	6.15	6.37	5.35
Cs	3.55	27.4	2.83	2.94	4.59	6.37	3.56
Ba	1040	1349	817	494	728	874	233
La	51.5	50.4	43.6	32.2	76.6	92.3	39.2
Ce	95.8	98.5	98	62	151	181	85.5
Pr	9.93	10.9	12	6.7	15.9	19.2	9.38
Nd	35.6	41	48.2	24.4	57.7	66.8	34
Sm	5.33	6.81	9.3	4.2	8.8	10.3	6.12
Eu	1.11	1.5	1.46	0.457	1.35	1.53	0.449
Gd	3.39	4.53	6.45	2.7	5.95	6.62	4.5
Tb	0.431	0.609	0.864	0.469	0.823	0.867	0.719
Dy	2.42	3.32	5.12	2.44	4.61	5.13	4.08
Ho	0.467	0.594	0.939	0.52	0.871	0.936	0.801
Er	1.21	1.62	2.57	1.19	2.36	2.52	2.37
Tm	0.163	0.22	0.37	0.2	0.342	0.335	0.342
Yb	1.13	1.34	2.42	1.37	2.08	2.64	2.15
Lu	0.179	0.185	0.38	0.237	0.355	0.37	0.312
Hf	5.3	5.82	7.9	3.9	7.36	7.39	5.17
Ta	0.854	0.848	1.79	1.68	1.53	1.42	1.72
Pb	14.6	16	21.9	20	25.4	23.1	25.4
Th	14.7	9.02	15.7	18.5	23.5	23.3	46.3
U	8.22	2.39	5.43	6.26	6.62	4.79	13.2
Eu/Eu*	0.75	0.78	0.55	0.39	0.54	0.53	0.25
Sr/Y	31.32	33.68	10.71	11.99	9.91	9.76	3.97
(La/Yb)n	32.69	26.98	12.92	16.86	26.42	25.08	13.08
10^4*(Ga/Al)	2.04	1.97	2.27	1.79	2.32	2.33	2.31
La_n/Sm_n	6.24	4.78	3.03	4.95	5.62	5.79	4.14
Gd_n/Yb_n	2.48	2.80	2.20	1.63	2.37	2.07	1.73

Analysis	U238/Pb206	Error (1σ)	Pb207/Pb206	Error (1σ)	Pb207/U235	Error (1σ)	Pb206/U238	Error (1σ)	Rho	Pb207/Pb206 Age (Ma)	Error (1σ)	Pb206/U238 Age (Ma)	Error (1σ)	Discordance (%)
XU-01A-2	2.049	0.018	0.178	0.002	11.964	0.119	0.488	0.004	0.903	**2633**	**18**	2562	19	2.68
XU-01A-10	2.590	0.022	0.176	0.002	9.370	0.101	0.386	0.003	0.780	**2616**	**20**	2105	15	19.54
XU-01A-11	2.291	0.020	0.178	0.002	10.687	0.107	0.437	0.004	0.857	**2630**	**19**	2335	17	11.23
XU-01A-13	2.051	0.018	0.178	0.002	11.940	0.124	0.488	0.004	0.839	**2631**	**19**	2560	18	2.68
XU-01A-14	1.984	0.018	0.177	0.002	12.294	0.131	0.504	0.004	0.832	**2625**	**20**	2631	19	-0.24
XU-01A-17	1.976	0.019	0.178	0.003	12.410	0.184	0.506	0.005	0.658	**2633**	**26**	2639	21	-0.22
XU-01A-18	1.976	0.017	0.178	0.002	12.398	0.131	0.506	0.004	0.817	**2632**	**20**	2640	19	-0.30
XU-01A-22	2.192	0.019	0.177	0.002	11.158	0.115	0.456	0.004	0.851	**2629**	**19**	2423	18	7.83
XU-01A-24	2.058	0.019	0.177	0.002	11.874	0.133	0.486	0.005	0.847	**2628**	**20**	2553	20	2.85
XU-01A-26	2.166	0.020	0.178	0.002	11.343	0.114	0.462	0.004	0.912	**2637**	**18**	2447	19	7.21
XU-01A-27	2.123	0.018	0.176	0.002	11.408	0.109	0.471	0.004	0.863	**2612**	**19**	2488	17	4.75
XU-01i-1	2.146	0.019	0.177	0.002	11.352	0.117	0.466	0.004	0.877	**2623**	**19**	2466	19	5.99
XU-01i-2	2.108	0.018	0.178	0.002	11.612	0.124	0.474	0.004	0.814	**2630**	**20**	2503	18	4.82
XU-01i-3	2.331	0.022	0.175	0.002	10.330	0.118	0.429	0.004	0.815	**2603**	**20**	2301	18	11.61
XU-01i-5	2.005	0.018	0.179	0.002	12.299	0.127	0.499	0.004	0.848	**2642**	**19**	2609	19	1.27
XU-01i-10	2.048	0.019	0.176	0.002	11.883	0.155	0.488	0.005	0.727	**2620**	**23**	2564	20	2.16
XU-01i-11	2.193	0.019	0.180	0.002	11.348	0.135	0.456	0.004	0.742	**2657**	**22**	2422	18	8.85
XU-01i-13	2.342	0.020	0.172	0.002	10.121	0.118	0.427	0.004	0.731	**2576**	**22**	2293	16	11.01
XU-01i-14	2.106	0.018	0.177	0.002	11.574	0.131	0.475	0.004	0.764	**2623**	**21**	2505	18	4.53
XU-01i-15	2.729	0.023	0.174	0.002	8.811	0.097	0.366	0.003	0.762	**2600**	**21**	2013	14	22.61
XU-01i-16	2.230	0.020	0.178	0.003	11.029	0.151	0.449	0.004	0.658	**2638**	**25**	2389	18	9.44
XU-01i-17	2.511	0.021	0.174	0.002	9.541	0.103	0.398	0.003	0.777	**2594**	**21**	2161	15	16.70
XU-01i-18	2.209	0.019	0.176	0.002	10.966	0.132	0.453	0.004	0.726	**2613**	**22**	2408	18	7.85
XU-01i-19	2.136	0.018	0.178	0.002	11.496	0.128	0.468	0.004	0.768	**2635**	**21**	2476	18	6.07
XU-01i-20	2.078	0.018	0.176	0.002	11.705	0.131	0.481	0.004	0.763	**2620**	**21**	2532	18	3.35
XU-01i-21	2.587	0.022	0.173	0.002	9.218	0.101	0.387	0.003	0.773	**2587**	**21**	2107	15	18.56
XU-02-3	2.311	0.018	0.181	0.002	10.774	0.107	0.433	0.003	0.782	**2658**	**20**	2318	15	12.80
XU-02-4	2.094	0.016	0.176	0.002	11.604	0.101	0.477	0.004	0.873	**2618**	**18**	2516	16	3.89
XU-02-6	2.076	0.016	0.176	0.002	11.674	0.098	0.482	0.004	0.898	**2613**	**18**	2535	16	2.99
XU-02-11	2.213	0.017	0.176	0.002	10.939	0.091	0.452	0.004	0.941	**2612**	**17**	2403	16	7.99
XU-02-12	2.320	0.018	0.177	0.002	10.512	0.090	0.431	0.003	0.909	**2624**	**18**	2310	15	11.96
XU-02-14	2.724	0.022	0.177	0.002	8.934	0.081	0.367	0.003	0.889	**2621**	**18**	2016	14	23.08

GP-01-1	2.130	0.017	0.177	0.002	11.461	0.105	0.469	0.004	0.873	**2626**	**19**	2481	16	5.50
GP-01-2	2.072	0.016	0.180	0.002	11.962	0.106	0.483	0.004	0.893	**2651**	**18**	2539	17	4.23
GP-01-4	1.937	0.016	0.180	0.002	12.801	0.118	0.516	0.004	0.873	**2651**	**19**	2684	18	-1.24
GP-01-5	1.943	0.016	0.180	0.002	12.749	0.118	0.515	0.004	0.888	**2650**	**18**	2677	18	-1.02
GP-01-6	1.909	0.015	0.179	0.002	12.933	0.115	0.524	0.004	0.900	**2644**	**18**	2716	18	-2.70
GP-01-7	2.099	0.016	0.181	0.002	11.887	0.110	0.476	0.004	0.820	**2662**	**19**	2511	16	5.66
GP-01-8	2.058	0.016	0.181	0.002	12.153	0.128	0.486	0.004	0.728	**2665**	**21**	2553	16	4.21
GP-01-9	1.927	0.016	0.185	0.002	13.208	0.118	0.519	0.004	0.905	**2694**	**18**	2695	18	-0.02
GP-01-10	1.990	0.016	0.179	0.002	12.386	0.108	0.503	0.004	0.914	**2642**	**18**	2625	17	0.64
GP-01-11	2.010	0.016	0.179	0.002	12.305	0.109	0.498	0.004	0.907	**2647**	**18**	2603	17	1.65
GP-01-12	2.047	0.016	0.180	0.002	12.137	0.104	0.489	0.004	0.923	**2654**	**17**	2565	17	3.38
GP-01-14	2.031	0.016	0.180	0.002	12.192	0.107	0.492	0.004	0.917	**2649**	**18**	2581	17	2.57
GP-01-15	2.071	0.017	0.179	0.002	11.899	0.106	0.483	0.004	0.905	**2641**	**18**	2540	17	3.83
GP-02-1	1.980	0.025	0.178	0.007	12.405	0.459	0.505	0.006	0.340	**2636**	**61**	2635	27	0.03
GP-02-8	1.997	0.029	0.180	0.009	12.445	0.604	0.501	0.007	0.304	**2656**	**81**	2617	32	1.45
GP-02-10	2.029	0.023	0.180	0.006	12.221	0.384	0.493	0.006	0.360	**2652**	**53**	2583	24	2.61
GP-02-11	2.129	0.031	0.180	0.009	11.630	0.524	0.470	0.007	0.319	**2649**	**76**	2482	30	6.29
GP-02-12	2.876	0.035	0.179	0.007	8.556	0.316	0.348	0.004	0.329	**2639**	**63**	1923	20	27.12
GP-02-14	3.464	0.045	0.175	0.008	6.956	0.284	0.289	0.004	0.317	**2604**	**70**	1635	19	37.21
GP-02-16	2.057	0.023	0.177	0.006	11.850	0.380	0.486	0.005	0.352	**2623**	**56**	2554	24	2.61
GP-02-17	1.967	0.023	0.178	0.006	12.478	0.408	0.508	0.006	0.352	**2635**	**57**	2650	25	-0.58
GP-02-19	2.004	0.023	0.177	0.006	12.146	0.390	0.499	0.006	0.353	**2621**	**56**	2610	24	0.41
GP-03-3	2.086	0.019	0.183	0.003	12.056	0.167	0.479	0.004	0.668	**2676**	**25**	2525	19	5.64
GP-03-4	1.956	0.017	0.181	0.002	12.747	0.123	0.511	0.005	0.918	**2661**	**18**	2662	19	-0.04
GP-03-16	1.954	0.018	0.176	0.002	12.447	0.147	0.512	0.005	0.799	**2620**	**21**	2664	21	-1.68
GP-03-17	2.140	0.018	0.183	0.002	11.794	0.115	0.467	0.004	0.881	**2681**	**19**	2472	18	7.79
GP-03-18	2.005	0.017	0.181	0.002	12.445	0.126	0.499	0.004	0.855	**2663**	**19**	2608	19	2.05
GP-03-20	2.040	0.017	0.181	0.002	12.203	0.113	0.490	0.004	0.926	**2658**	**18**	2572	18	3.25
GP-03-21	2.031	0.017	0.181	0.002	12.298	0.117	0.492	0.004	0.895	**2664**	**18**	2581	18	3.09
GX-01-3	2.819681	0.024011	0.17313	0.00241	8.46407	0.10478	0.35465	0.00302	0.687872	**2588**	**23**	1957	14	24.39
GX-01-4	8.085382	0.067988	0.15076	0.00208	2.57041	0.03155	0.12368	0.00104	0.685073	**2355**	**23**	752	6	68.08
GX-01-5	6.442054	0.05644	0.16327	0.00212	3.49363	0.04102	0.15523	0.00136	0.746182	**2490**	**22**	930	8	62.64
GX-01-6	6.299609	0.054765	0.15778	0.00238	3.45275	0.04733	0.15874	0.00138	0.634193	**2432**	**25**	950	8	60.95

GX-01-7	3.644846	0.033079	0.16341	0.00258	6.18021	0.09037	0.27436	0.00249	0.620665	**2491**	**26**	1563	13	37.27
GX-01-9	4.322455	0.03718	0.15905	0.00212	5.07247	0.06075	0.23135	0.00199	0.718219	**2446**	**22**	1342	10	45.14
GX-01-10	7.35132	0.063229	0.16024	0.00262	3.00473	0.04477	0.13603	0.00117	0.577257	**2458**	**27**	822	7	66.55
GX-01-12	6.517205	0.062861	0.16647	0.00306	3.52129	0.06141	0.15344	0.00148	0.553077	**2523**	**31**	920	8	63.52
GX-01-13	4.703226	0.041586	0.17342	0.00298	5.08274	0.08041	0.21262	0.00188	0.55891	**2591**	**28**	1243	10	52.04
GX-01-14	5.737235	0.05102	0.15941	0.00226	3.83016	0.04991	0.1743	0.00155	0.682439	**2449**	**24**	1036	9	57.72
GX-01-16	2.769239	0.023926	0.1796	0.00278	8.94069	0.12595	0.36111	0.00312	0.613321	**2649**	**25**	1987	15	24.98
GX-01-18	2.197609	0.020042	0.17754	0.00297	11.13743	0.17337	0.45504	0.00415	0.585881	**2630**	**28**	2418	18	8.08
GX-01-22	2.75247	0.024774	0.17352	0.00288	8.69091	0.13443	0.36331	0.00327	0.581888	**2592**	**27**	1998	15	22.92
GX-01-23	2.372648	0.021617	0.17841	0.0026	10.36672	0.14046	0.42147	0.00384	0.67244	**2638**	**24**	2267	17	14.06
GX-01-24	5.348166	0.048339	0.1607	0.00289	4.14226	0.06962	0.18698	0.00169	0.537768	**2463**	**30**	1105	9	55.14
GX-01-25	6.85777	0.060667	0.15168	0.0028	3.04906	0.05241	0.14582	0.00129	0.514665	**2365**	**31**	878	7	62.89
GX-01-27	3.996643	0.04185	0.17695	0.00482	6.1033	0.15967	0.25021	0.00262	0.400256	**2625**	**45**	1440	14	45.15

Analyses no.	$^{176}Lu/^{177}Hf$	1 σ	$^{176}Hf/^{177}Hf$	1 σ	$^{176}Hf/^{177}Hf_i$	2 σ	εHf $_0$	εHf $_i$	2 σ	Domain
XU-01										
XU01-1	0.000842	0.000015	0.281130	0.000009	0.281088	0.00002	-58.51	-0.14	0.32	rim
XU01-2	0.000422	0.000001	0.281109	0.000008	0.281088	0.00002	-59.25	-0.14	0.28	metamict core
XU01-3	0.001007	0.000004	0.281174	0.000006	0.281124	0.00001	-56.95	1.13	0.21	metamict core
XU01-4	0.000423	0.000001	0.281113	0.000008	0.281092	0.00002	-59.11	0.01	0.28	rim
XU01-5	0.000302	0.000002	0.281106	0.000007	0.281091	0.00001	-59.36	-0.03	0.25	rim
XU01-6	0.000612	0.000007	0.281128	0.000007	0.281098	0.00001	-58.58	0.20	0.25	core
XU01-7	0.000446	0.000003	0.281124	0.000007	0.281102	0.00001	-58.72	0.36	0.25	rim
XU01-8	0.000677	0.000017	0.281134	0.000009	0.281100	0.00002	-58.37	0.30	0.32	core
XU01-9	0.000480	0.000002	0.281117	0.000007	0.281093	0.00001	-58.97	0.05	0.25	rim
XU-01A										
XU01A-1	0.000630	0.000008	0.281120	0.000007	0.281089	0.00001	-58.86	-0.19	0.25	core
XU01A-2	0.000370	0.000004	0.281110	0.000007	0.281092	0.00001	-59.22	-0.08	0.25	rim
XU01A-3	0.001431	0.000038	0.281195	0.000009	0.281123	0.00002	-56.21	1.05	0.32	metamict core
XU01A-4	0.000639	0.000002	0.281124	0.00001	0.281092	0.00002	-58.72	-0.06	0.36	rim
XU01A-5	0.000720	0.000022	0.281124	0.000009	0.281088	0.00002	-58.72	-0.20	0.32	core
XU01A-6	0.000562	0.000019	0.281119	0.000007	0.281091	0.00001	-58.90	-0.10	0.25	metamict core
XU01A-7	0.000513	0.000003	0.281120	0.000007	0.281095	0.00001	-58.86	0.02	0.25	rim
XU-02										
XU02-1	0.000599	0.000002	0.281119	0.000014	0.281090	0.00003	-58.90	-0.46	0.50	rim
XU02-2	0.001262	0.000018	0.281169	0.000009	0.281106	0.00002	-57.13	0.13	0.32	metamict core
XU02-3	0.002112	0.000035	0.281274	0.000011	0.281168	0.00002	-53.45	2.32	0.39	metamict core
XU02-4	0.000578	0.000006	0.281132	0.000008	0.281104	0.00002	-58.44	0.04	0.28	rim
GP-01										
GP01-1	0.001421	0.000022	0.281187	0.000013	0.281115	0.00003	-56.49	1.41	0.46	metamict core
GP01-2	0.000914	0.000013	0.281135	0.00001	0.281089	0.00002	-58.33	0.48	0.36	rim
GP01-3	0.001146	0.000006	0.281150	0.00001	0.281092	0.00002	-57.80	0.59	0.36	core
GP01-4	0.001141	0.000003	0.281142	0.000012	0.281084	0.00002	-58.08	0.32	0.43	rim
GP01-5	0.000957	0.000019	0.281127	0.000009	0.281079	0.00002	-58.61	0.12	0.32	metamict core
GP01-6	0.000583	0.000011	0.281116	0.000009	0.281087	0.00002	-59.00	0.40	0.32	rim
GP01-7	0.000783	0.000005	0.281134	0.000009	0.281095	0.00002	-58.37	0.68	0.32	core
GP01-8	0.000190	0.000004	0.281090	0.000008	0.281081	0.00002	-59.92	0.19	0.28	rim
GP-02										
GP02-1	0.000877	0.000038	0.281148	0.000009	0.281104	0.00002	-57.87	0.46	0.32	metamict core
GP02-2	0.000565	0.000007	0.281117	0.000009	0.281089	0.00002	-58.97	-0.08	0.32	rim
GP02-3	0.000768	0.000025	0.281134	0.000009	0.281096	0.00002	-58.37	0.16	0.32	metamict core
GP02-4	0.000718	0.000007	0.281130	0.000009	0.281094	0.00002	-58.51	0.11	0.32	rim
GP02-5	0.000648	0.000007	0.281126	0.000007	0.281094	0.00001	-58.65	0.09	0.25	core
GP02-6	0.000782	0.000006	0.281155	0.000008	0.281116	0.00002	-57.62	0.88	0.28	rim
GP02-7	0.000889	0.000022	0.281127	0.000009	0.281083	0.00002	-58.61	-0.31	0.32	core
GP02-8	0.000388	0.000002	0.281099	0.000007	0.281080	0.00001	-59.60	-0.41	0.25	rim
GP-03										
GP03-1	0.001159	0.000013	0.281143	0.00001	0.281085	0.00002	-58.05	0.09	0.36	rim
GP03-2	0.000693	0.000044	0.281127	0.000009	0.281092	0.00002	-58.61	0.36	0.32	core
GP03-3	0.000802	0.000016	0.281109	0.000009	0.281069	0.00002	-59.25	-0.47	0.32	rim
GP03-4	0.001325	0.000026	0.281123	0.000012	0.281056	0.00002	-58.76	-0.92	0.43	rim
GP03-5	0.000444	0.000008	0.281085	0.000008	0.281063	0.00002	-60.10	-0.68	0.28	rim
GP03-6	0.000941	0.000057	0.281115	0.000007	0.281068	0.00001	-59.04	-0.51	0.25	rim
GP03-7	0.000621	0.000007	0.281120	0.00001	0.281089	0.00002	-58.86	0.24	0.36	metamict core
GP03-8	0.000970	0.000015	0.281120	0.00001	0.281071	0.00002	-58.86	-0.38	0.36	rim
GX-01										
GX01-1	0.000962	0.000038	0.281134	0.000009	0.281086	0.00002	-58.37	-0.01	0.32	metamict core
GX01-2	0.000877	0.000008	0.281153	0.000008	0.281109	0.00002	-57.69	0.82	0.28	rim
GX01-3	0.000910	0.000011	0.281135	0.00001	0.281089	0.00002	-58.33	0.12	0.36	core
GX01-4	0.001134	0.000013	0.281151	0.00001	0.281094	0.00002	-57.77	0.29	0.36	rim
GX01-5	0.003061	0.000033	0.281276	0.000015	0.281121	0.00003	-53.38	1.23	0.53	metamict core
GX01-6	0.000563	0.000011	0.281130	0.000008	0.281102	0.00002	-58.51	0.57	0.28	rim
GX01-7	0.001432	0.000035	0.281239	0.00001	0.281167	0.00002	-54.65	2.88	0.36	metamict core
GX01-8	0.001387	0.000031	0.281207	0.000011	0.281137	0.00002	-55.78	1.82	0.39	rim

Figure captions

Figure 1

Simplified geological map of Tanzania showing the main tectonic units and terrane boundaries as proposed by Kabete et al., (2012a). Inset map of Africa showing distribution of Archean crust and the location of Tanzania craton.

Figure 2

Simplified geological map of Geita Greenstone Belt showing the main geological units and the location of the samples used in this study.

Figure 3

Cathodoluminescence images of representative zircon grains from each sample. a) Sample XU-01; b) Sample XU-01A; c) Sample XU-02; d) Sample GP-01; e) Sample GP-02; f) Sample GP-03; g) Sample GX-01.

Figure 4

Normative An-Ab-Or diagram (a) showing the distribution of samples into the granite and granodiorite fields and Al_2O_3-Na_2O-K_2O diagram (b) showing the sodic-ptassic and peraluminous character of the samples.

Figure 5

Harker diagrams showing the compositional variation of major elements for Sukumaland granites (open circles) and Musoma Mara granites (triangles – Manya et al., 2007; crosses - Mshiu and Maboko, 2012).

Figure 6

Diagram (a) showing the variation of Eu/Eu* vs SiO_2 for Sukumaland granites (open circles) and for Musoma Mara granites (triangles – Manya et al., 2007; crosses - Mshiu and Maboko, 2012). b) Chondrite normalized REE diagram for Sukumaland granites. Shaded area shows the chondrite normalized pattern for Musoma Mara granites (Manya et al., 2007; Mshiu and Maboko, 2012). Normalizing values from Sun and McDonough (1989).

Figure 7

Diagrams showing the $^{207}Pb/^{206}Pb$ weighted average ages and concordia plots for all samples. a and b) Sample XU-01; c and d) Sample XU-01A; e and f) Sample XU-02; g and h) Sample GP-01; i and j) Sample GP-02; k and l) Sample GP-03; m) Sample GX-01.

Figure 8

Diagrams showing the Lu-Hf isotope data for the granites south of Lake Victoria. a) density probability plot showing that $^{176}Hf/^{177}Hf$ ratio for all samples have a uniform distribution; b) density probability plot showing that εHf vaules for all sample have a uniform distribution and plot near the CHUR vaule of 0; c) plot of $^{176}Hf/^{177}Hf$ versus the assumed crystallization ages; d) plot of εHf versus the assumed crystallization ages.

Figure 9

Probability distribution plots showing the distribution of a) plutonic ages in Sukumaland Greenstone belt; b) volcanic ages in Sukumaland Greenstone Belt; c) plutonic ages in Musoma Mara Greenstone Belt and d) volcanic ages in Musoma Mara Greenstone Belt.

Figure 10

Probability density diagrams showing the distribution of a) plutonic ages in Tanzania Craton; b) volcanic ages in Tanzania Craton; c) reworked Archean ages from the surrounding mobile belts and d) all available Archean ages for the Tanzania Craton.

Figure 11

Diagram showing the primitive mantle normalized trace elements concentration for Sukumaland granites and for Musoma Mara granites (Manya et al., 2007; Mshiu and Maboko, 2012). Normalizing values from Sun and McDonough (1989).

Table captions

Table 1

Major element composition for Sukumaland granites. ASI- aluminum saturation index.

Table 2

Trace element composition (ppm) for Sukumaland granites.

Table 3

Table showing the analytical results and the calculated ages for all samples. Only the analytical spots used in the age calculations are shown.

Table 4

Lu-Hf isotope data and time corrected parameters of zircon in granites from south of Lake Victoria.

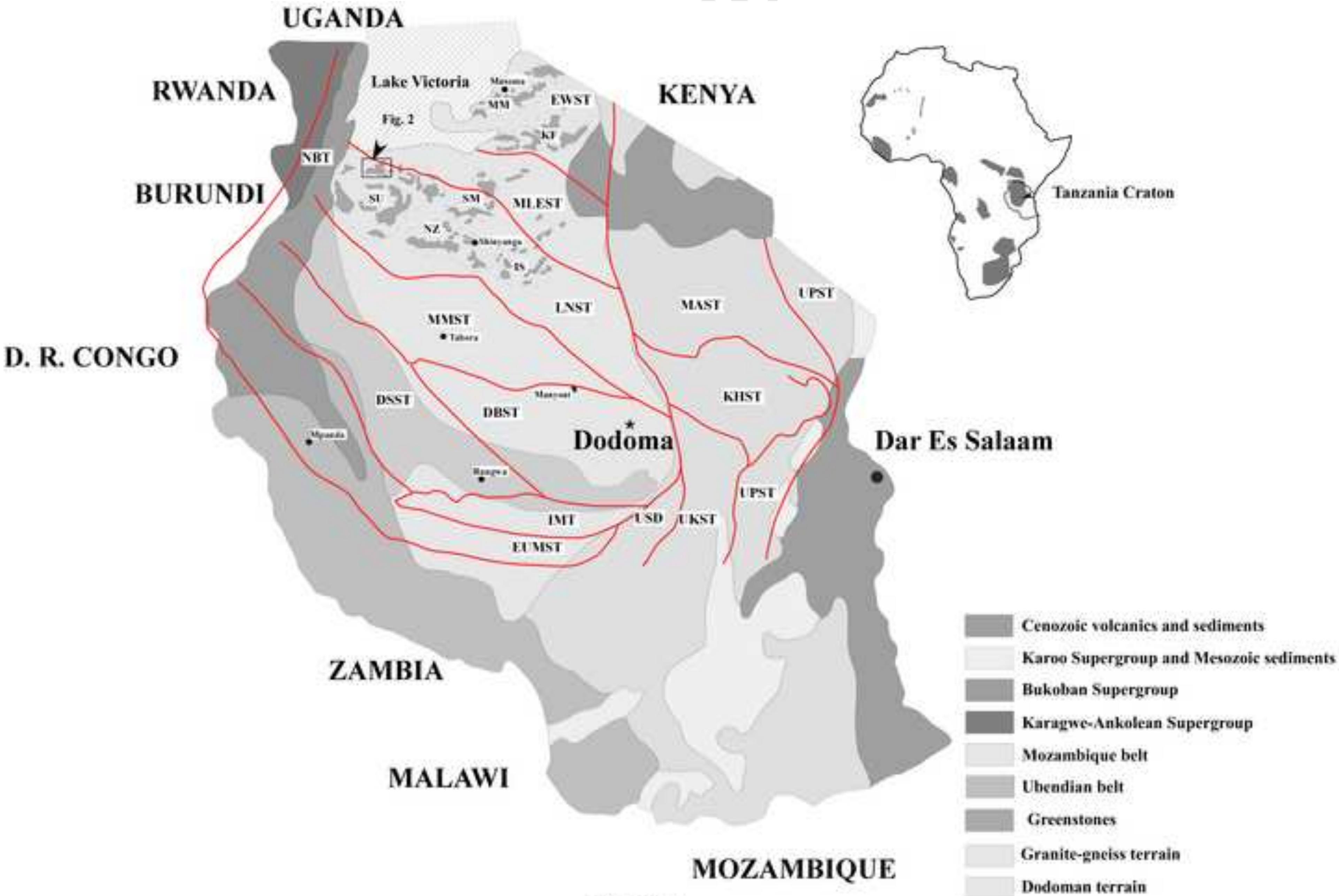
UGANDA
RWANDA
BURUNDI
D. R. CONGO
KENYA
ZAMBIA
MALAWI
MOZAMBIQUE
Lake Victoria
Fig. 2
NBT
MM
EWST
KF
SU
SM
MLEST
NZ
IS
MMST
LNST
MAST
UPST
DSST
DBST
KHST
Dodoma
Dar Es Salaam
UPST
IMT
USD
UKST
EUMST
Tanzania Craton
Cenozoic volcanics and sediments
Karoo Supergroup and Mesozoic sediments
Bukoban Supergroup
Karagwe-Ankolean Supergroup
Mozambique belt
Ubendian belt
Greenstones
Granite-gneiss terrain
Dodoman terrain

Figure 1

Figure

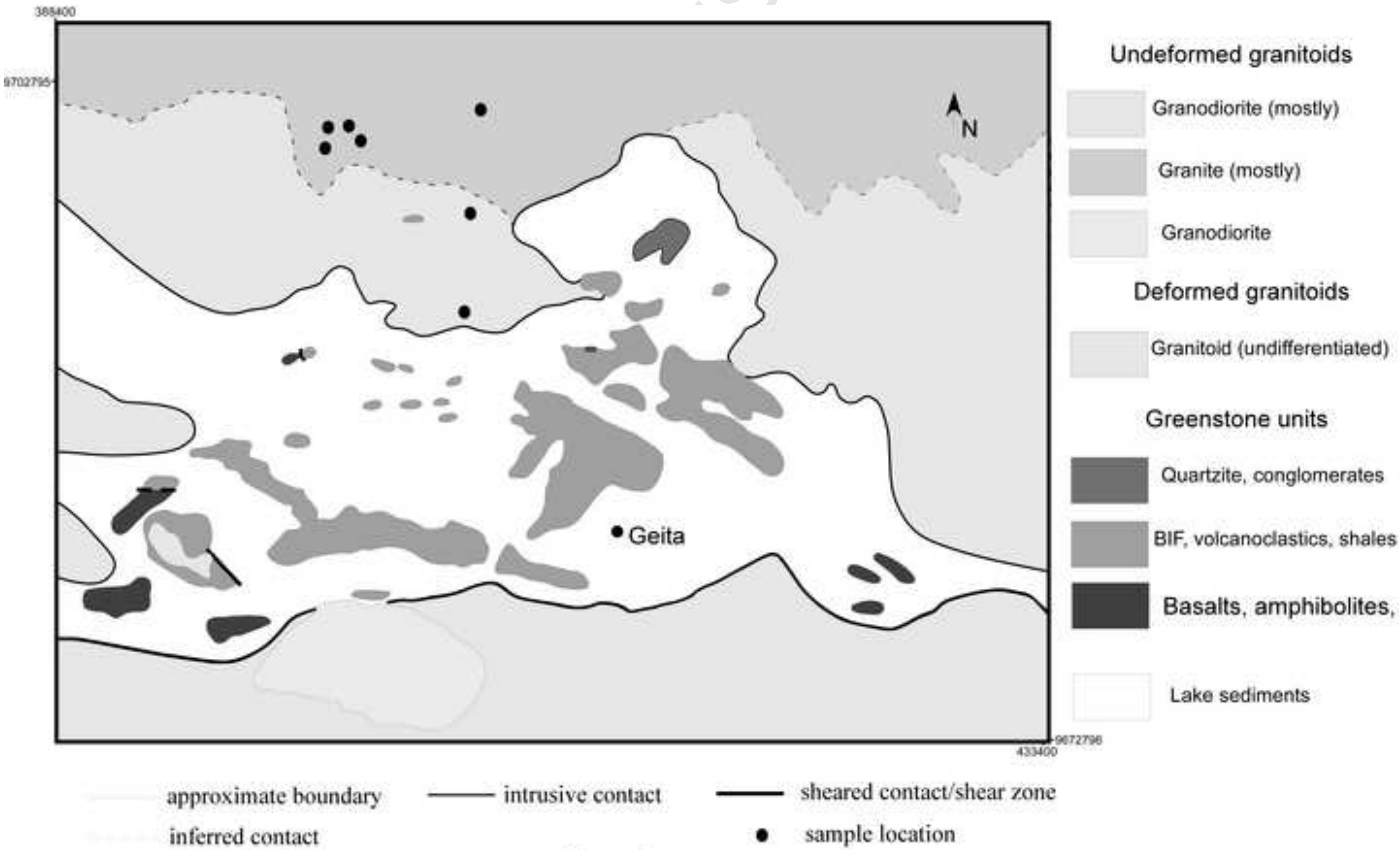

Figure 2

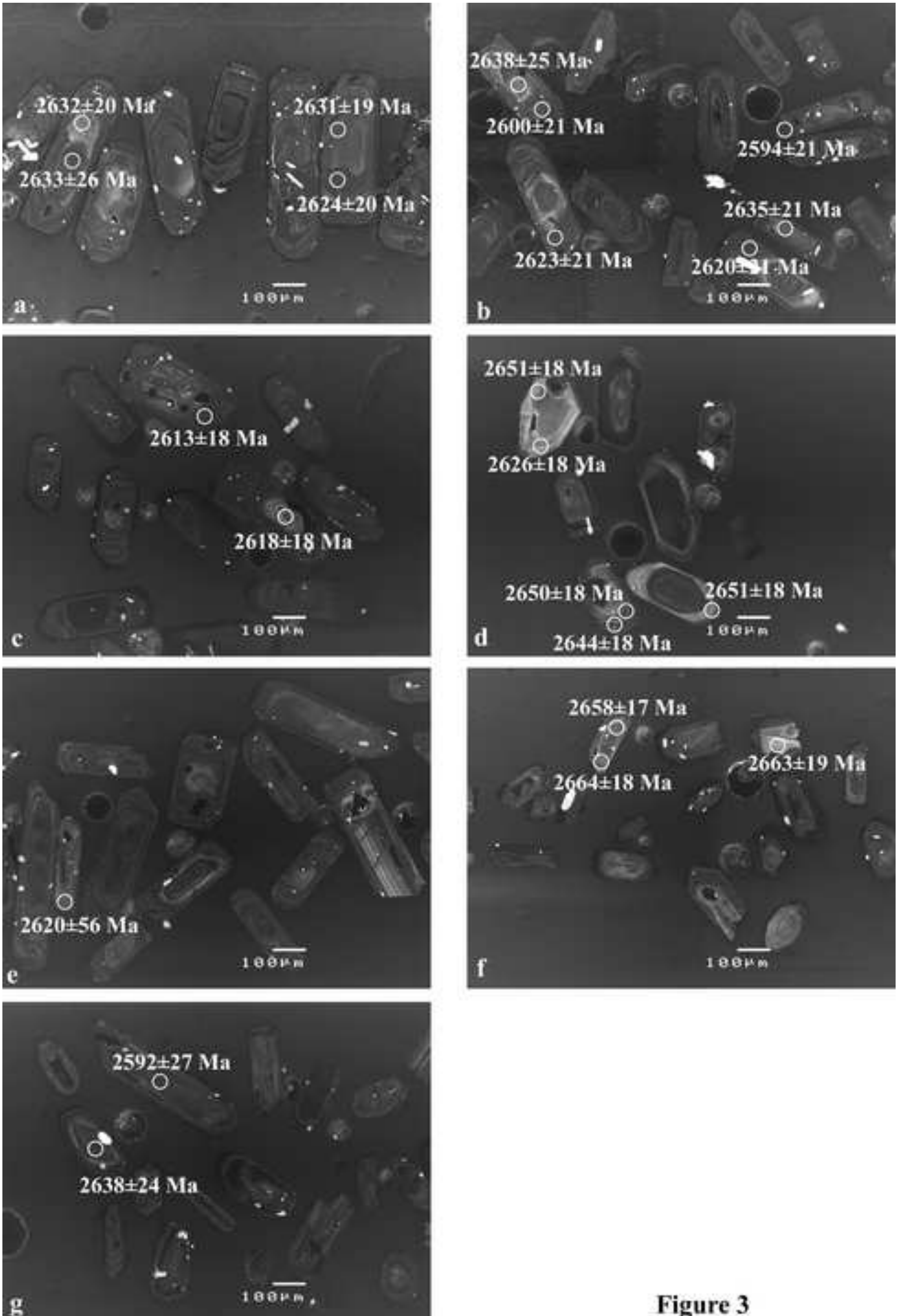
2632±20 Ma
2631±19 Ma
2633±26 Ma
2624±20 Ma
100μm
a
2638±25 Ma
2600±21 Ma
2594±21 Ma
2635±21 Ma
2623±21 Ma
100μm
b
2613±18 Ma
2618±18 Ma
100μm
c
2651±18 Ma
2626±18 Ma
2650±18 Ma
2651±18 Ma
2644±18 Ma
100μm
d
2620±56 Ma
100μm
e
2658±17 Ma
2663±19 Ma
2664±18 Ma
100μm
f
2592±27 Ma
2638±24 Ma
100μm
g

Figure 3

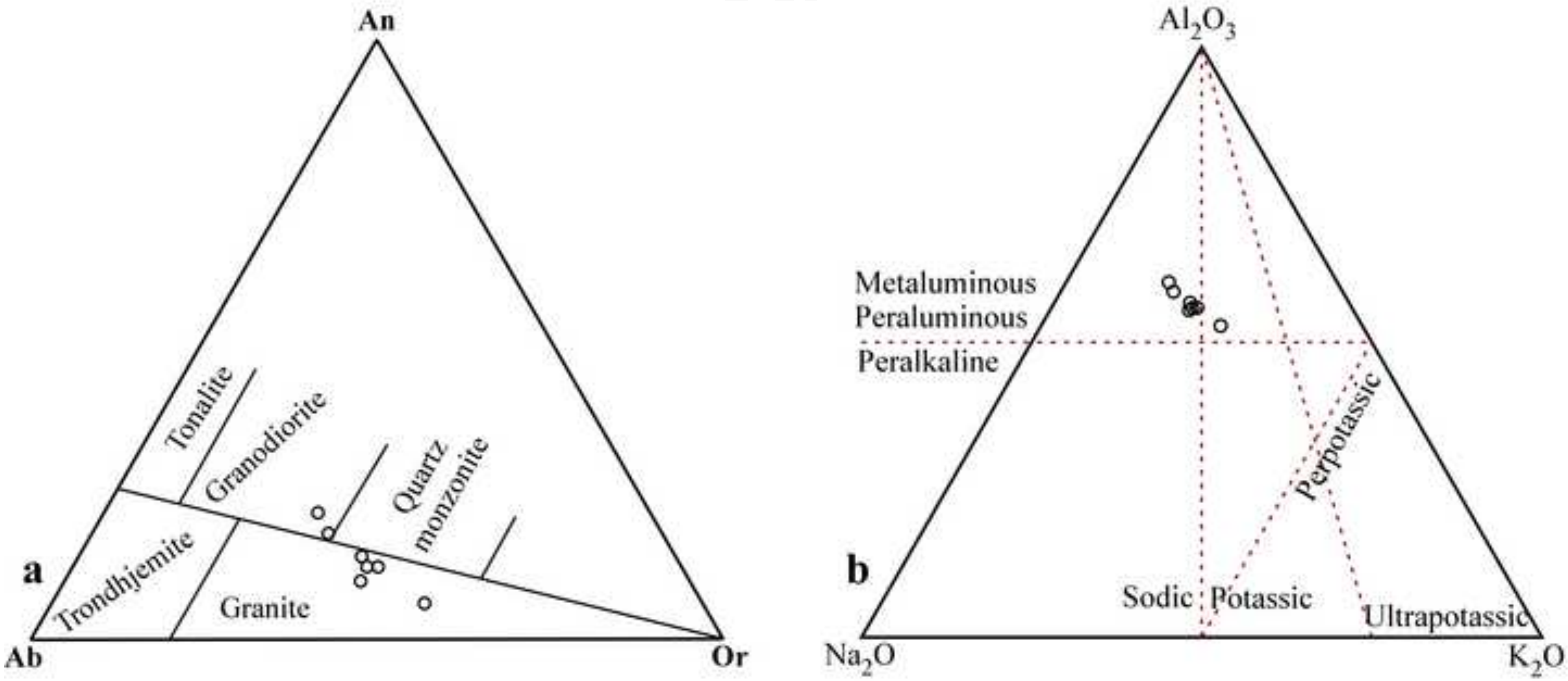
An
Tonalite
Granodiorite
Quartz monzonite
Trondhjemite
Granite
a
Ab
Or
Al_2O_3
Metaluminous
Peraluminous
Peralkaline
Perpotassic
b
Sodic
Potassic
Ultrapotassic
Na_2O
K_2O

Figure 4

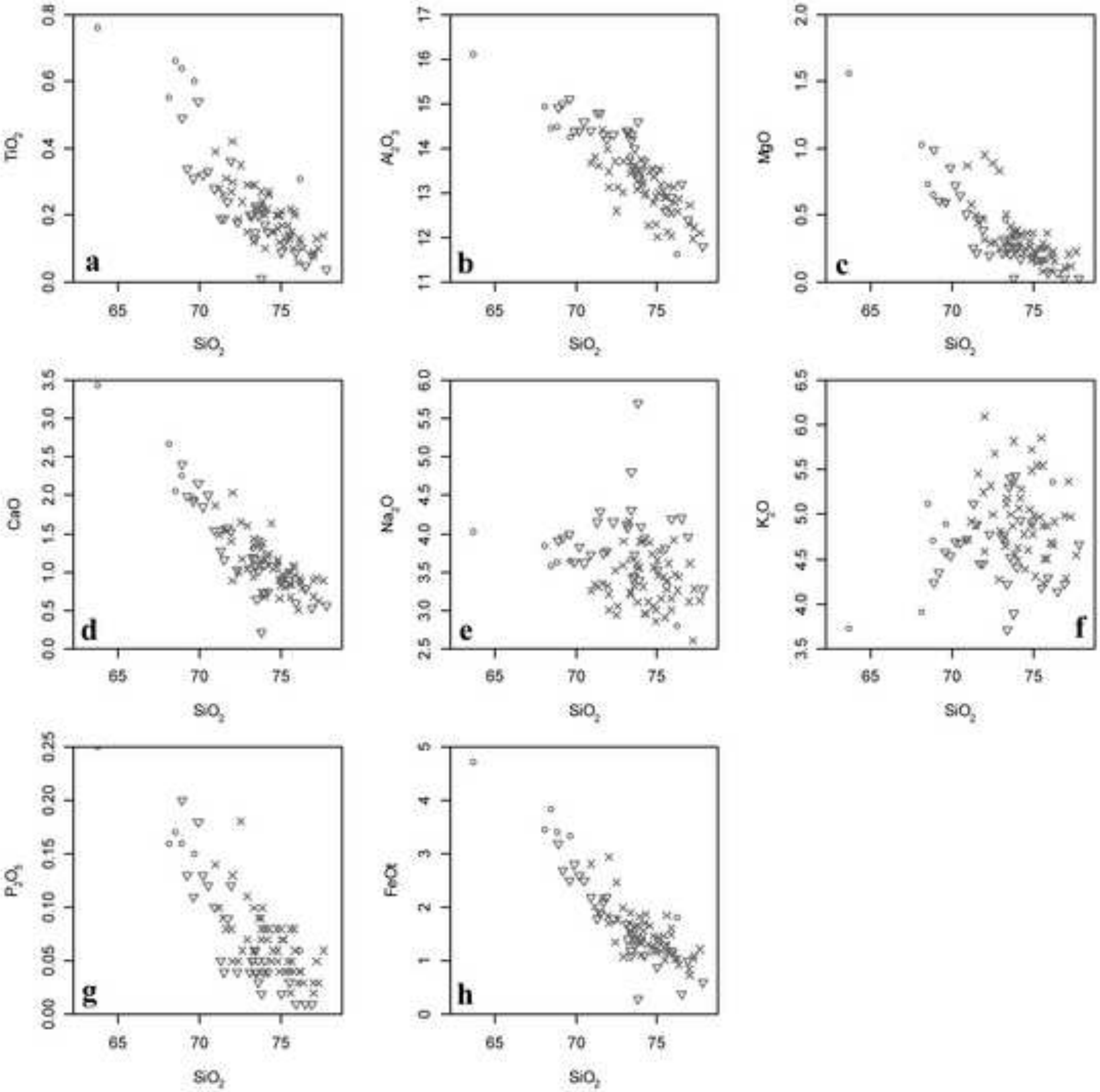

Figure 5

Figure

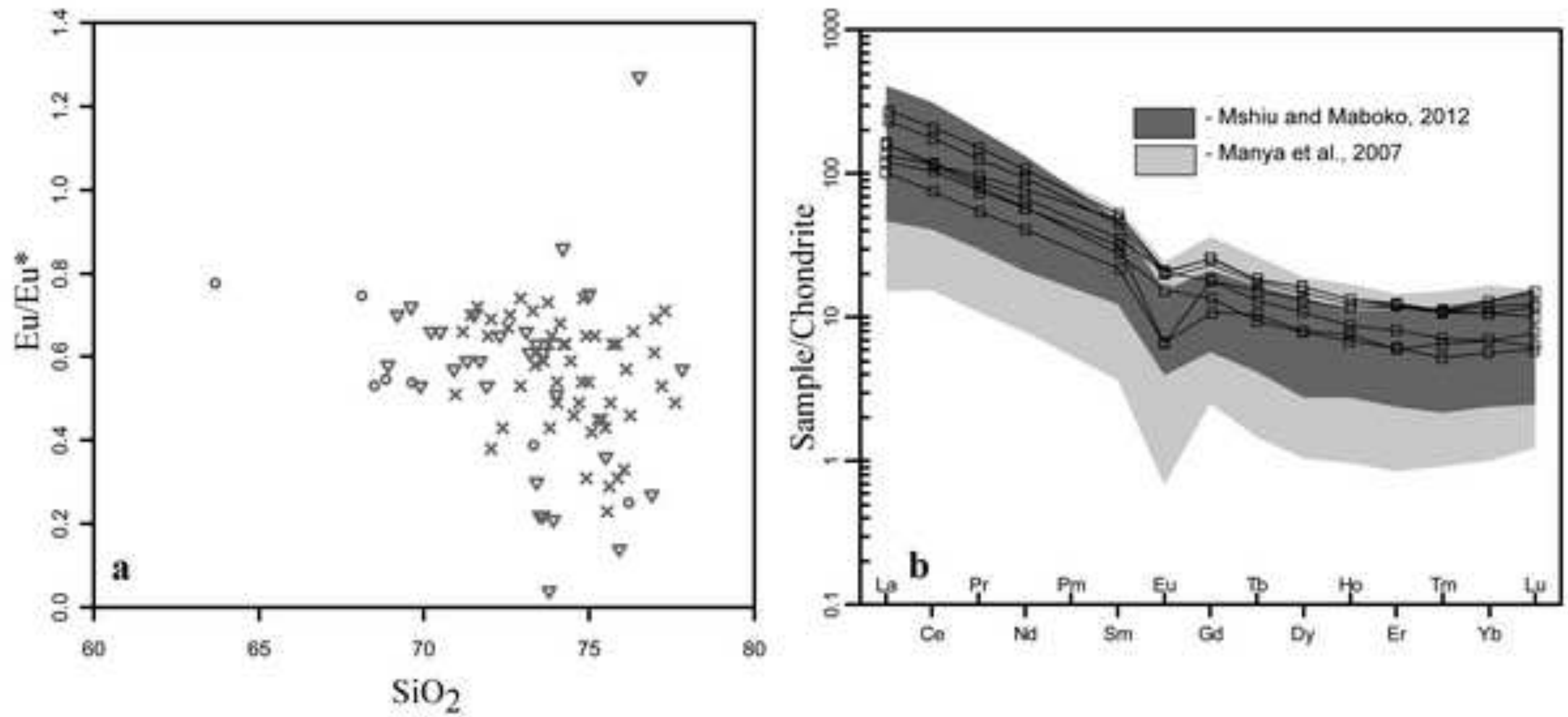

Figure 6

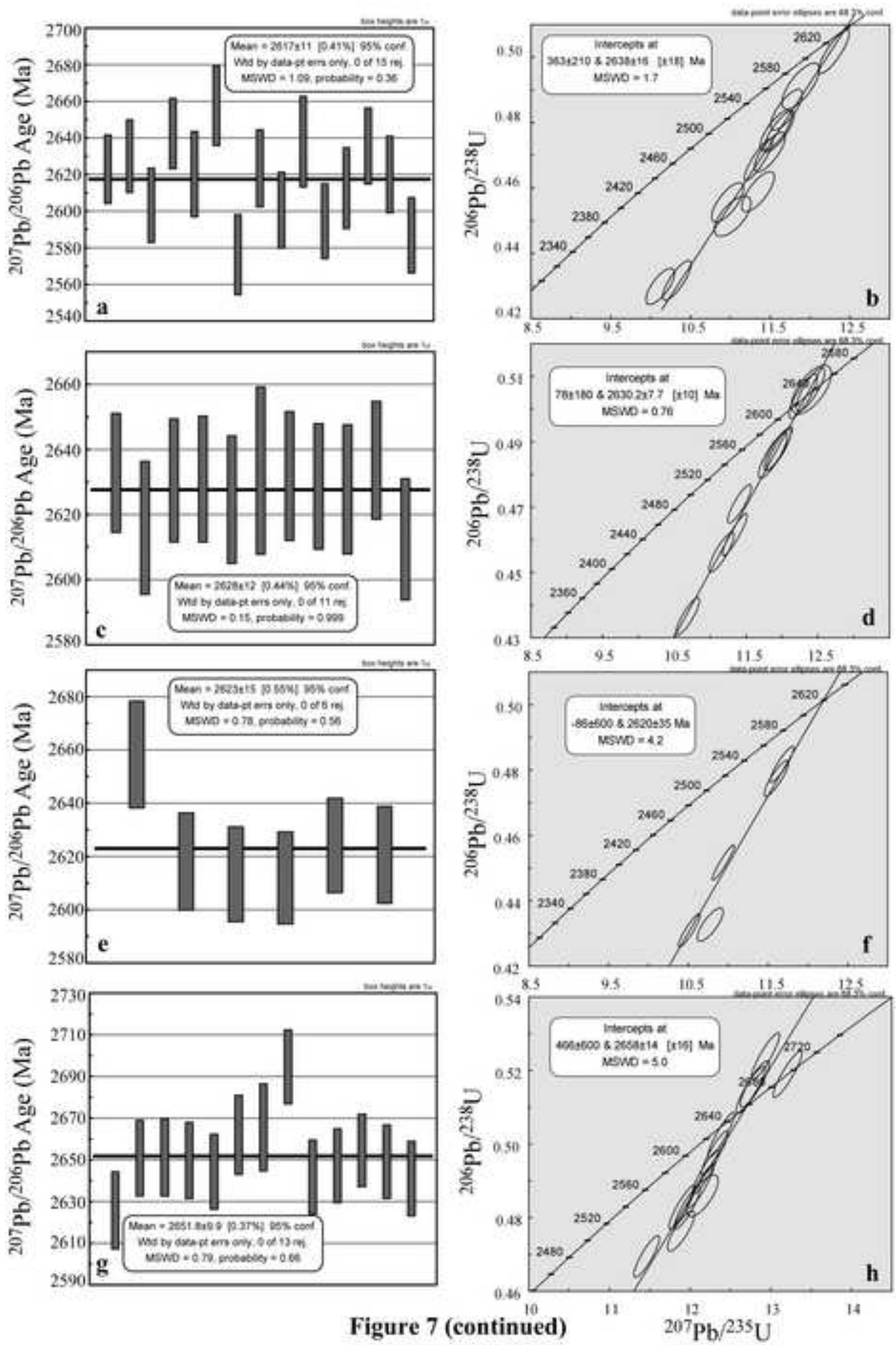

Figure 7 (continued)

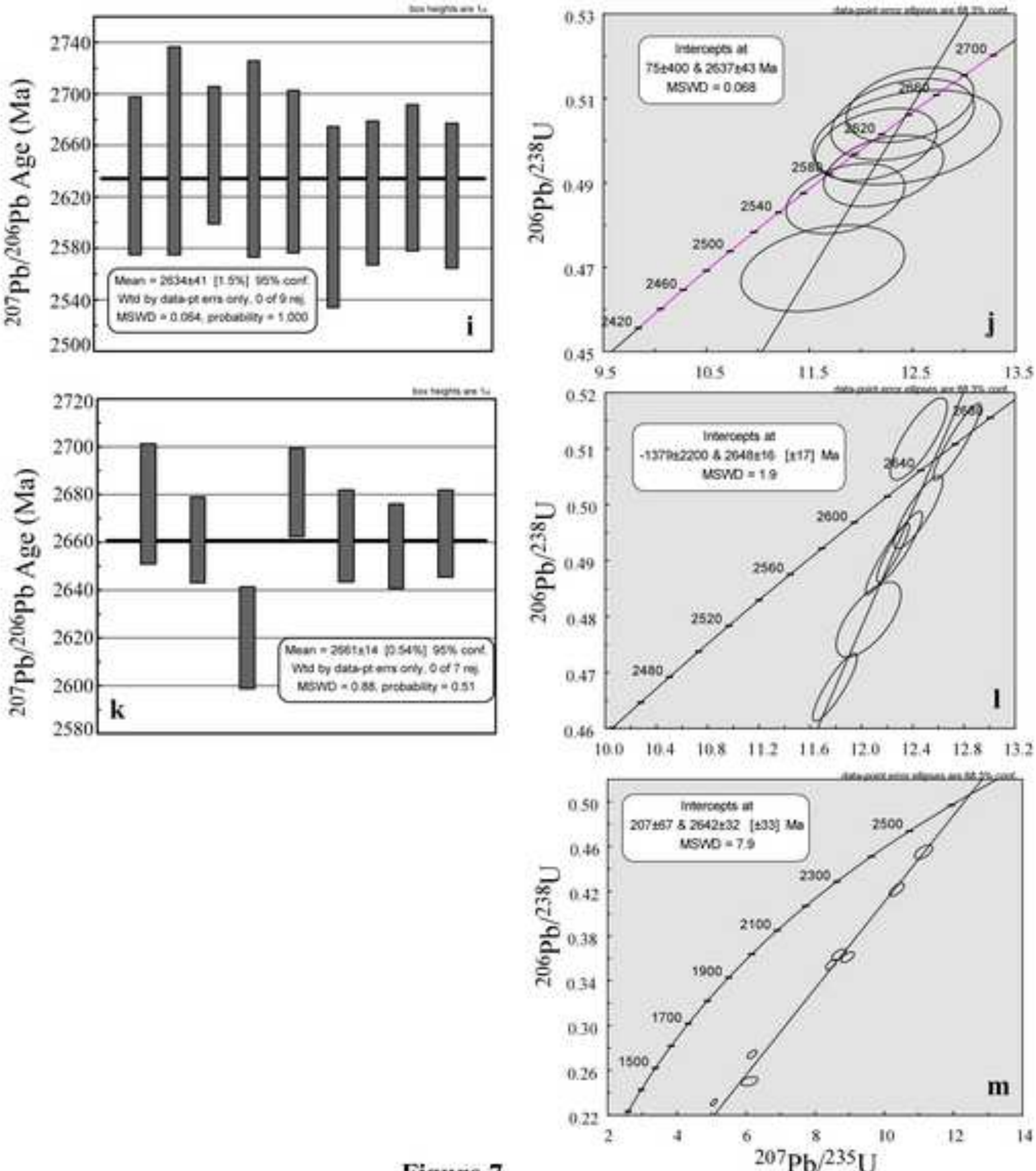

$^{207}Pb/^{206}Pb$ Age (Ma)
Mean = 2634±41 [1.5%] 95% conf.
Wtd by data-pt errs only, 0 of 9 rej.
MSWD = 0.064, probability = 1.000
i
Intercepts at
75±400 & 2637±43 Ma
MSWD = 0.068
j
Mean = 2661±14 [0.54%] 95% conf.
Wtd by data-pt errs only, 0 of 7 rej.
MSWD = 0.88, probability = 0.51
k
Intercepts at
-1379±2200 & 2648±16 [±17] Ma
MSWD = 1.9
l
Intercepts at
207±67 & 2642±32 [±33] Ma
MSWD = 7.9
m
$^{206}Pb/^{238}U$
$^{207}Pb/^{235}U$

Figure 7

Figure

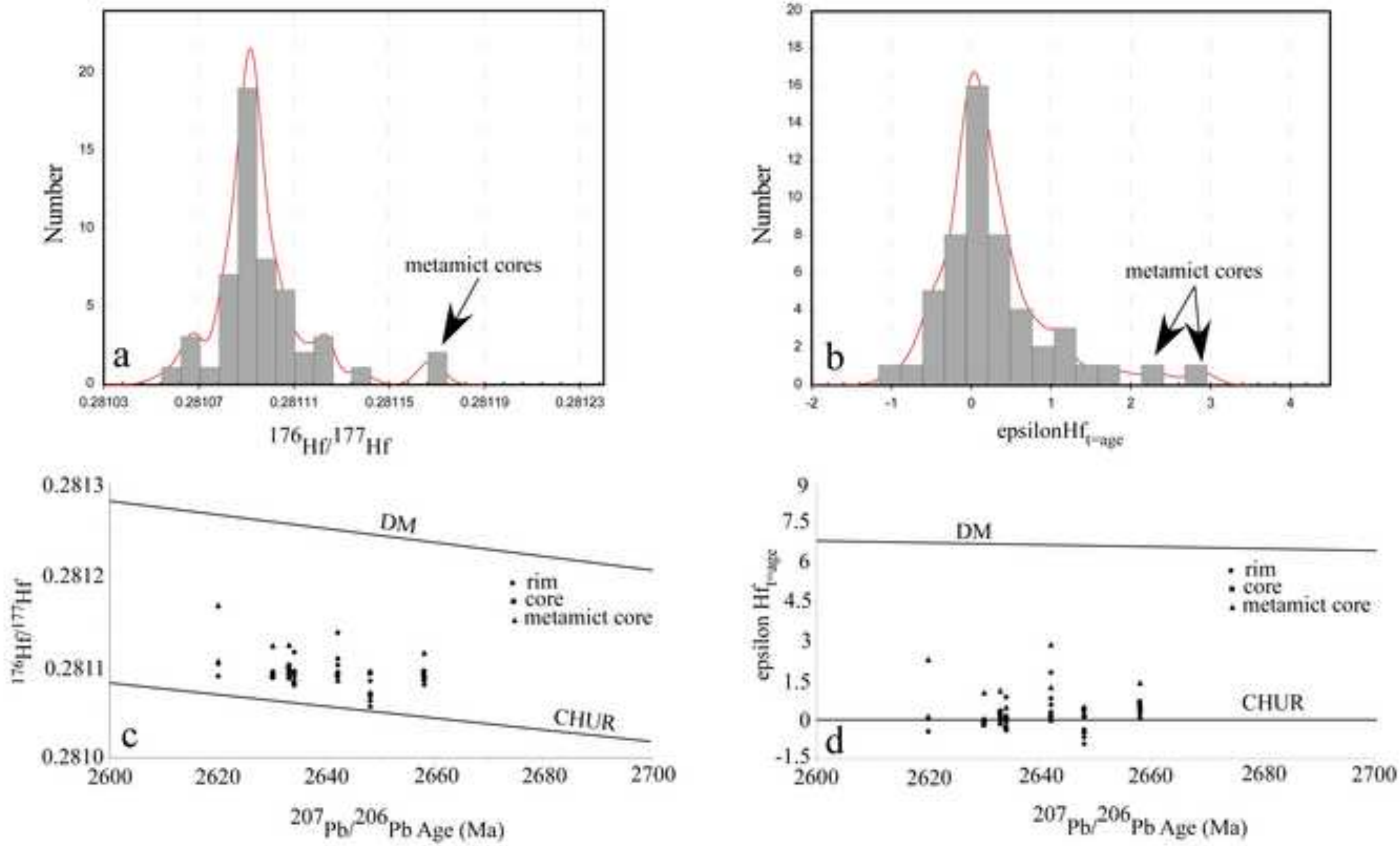

Figure 8

Figure

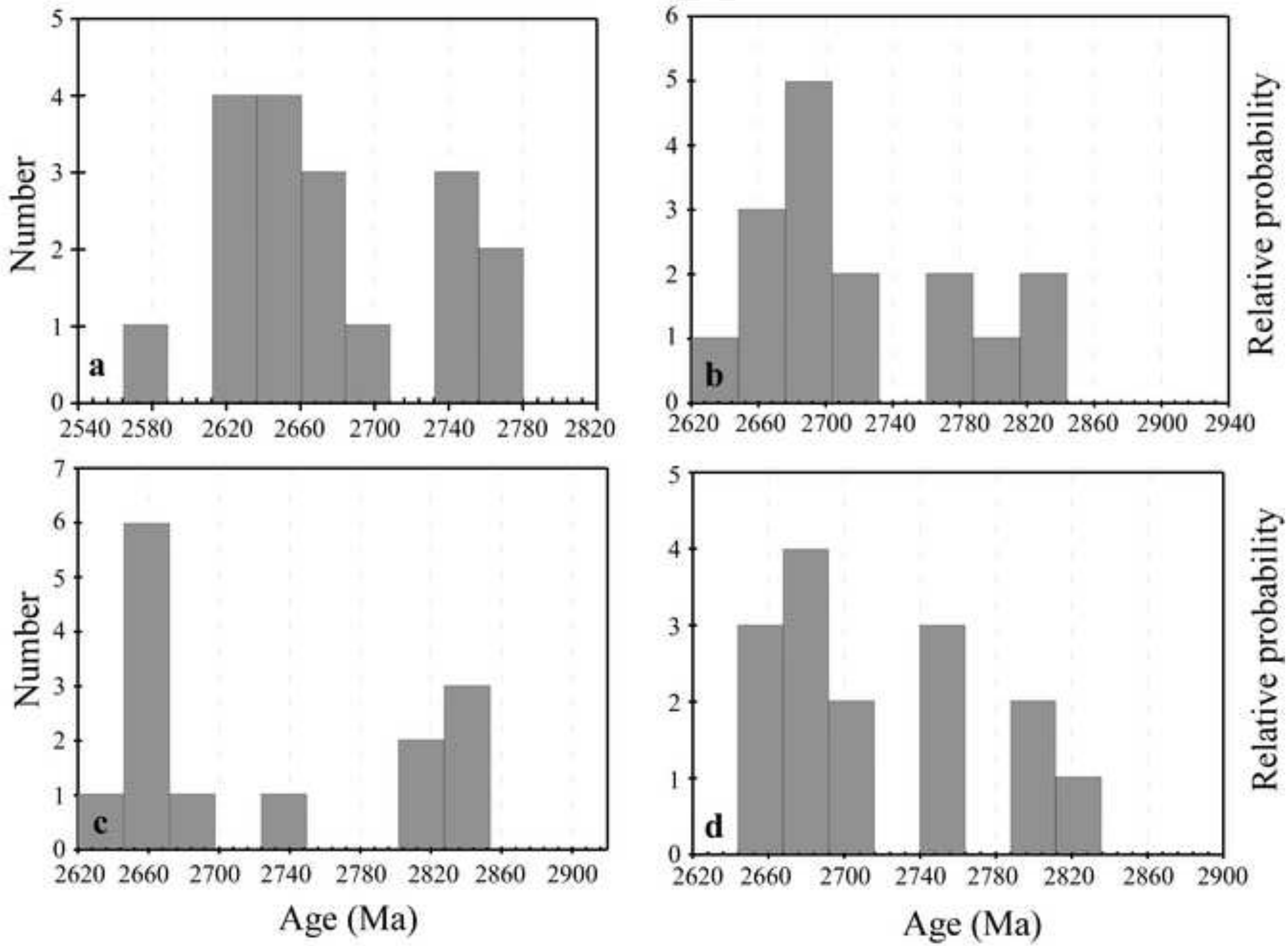

Figure 9

Figure

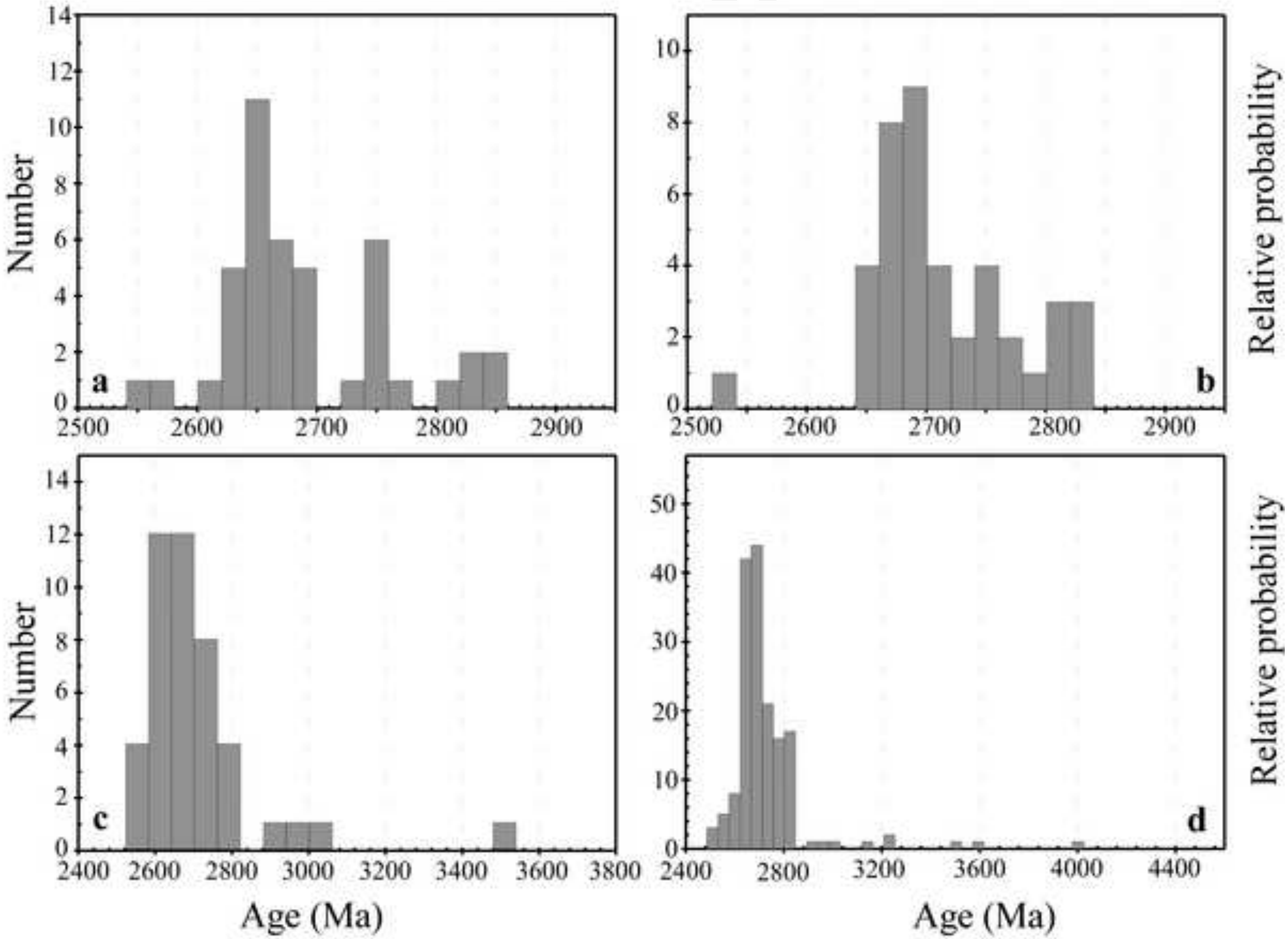

Figure 10

Figure

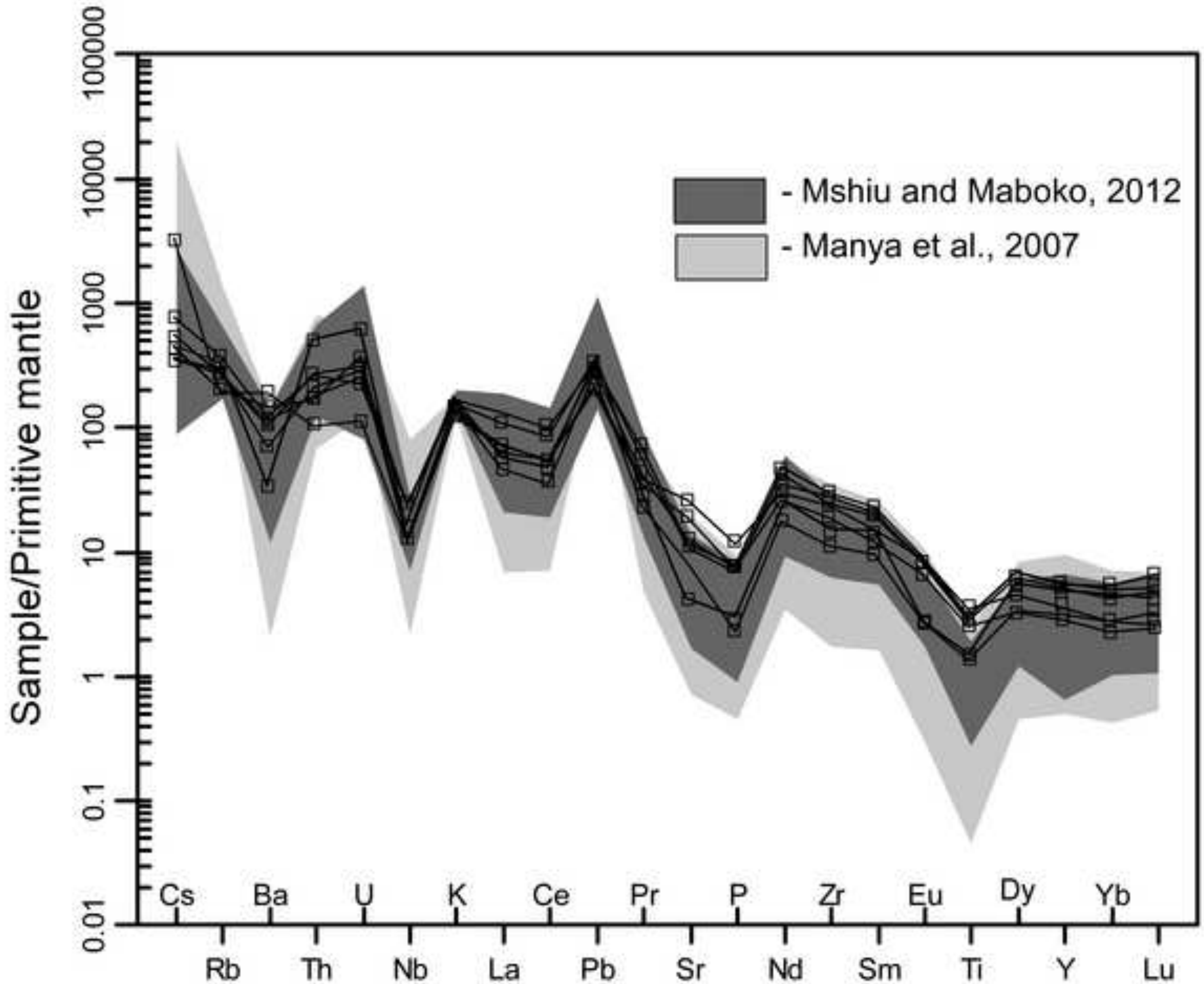

Figure 11